Title
Formation and transport of oxidized reactive nitrogen, ozone, and secondary organic aerosol in Tokyo

Journal
Journal of Geophysical Research Atmospheres, 113(21)

ISSN
0148-0227

Authors
Kondo, Y
Morino, Y
Fukuda, M
et al.

Publication Date
2008-11-16

DOI
10.1029/2008JD010134

Formation and transport of oxidized reactive nitrogen, ozone, and secondary organic aerosol in Tokyo

Y. Kondo,[1] Y. Morino,[2] M. Fukuda,[1] Y. Kanaya,[3] Y. Miyazaki,[1,4] N. Takegawa,[1] H. Tanimoto,[2] R. McKenzie,[5] P. Johnston,[5] D. R. Blake,[6] T. Murayama,[7] and M. Koike[8]

Received 16 March 2008; revised 30 July 2008; accepted 7 August 2008; published 13 November 2008.

[1] Measurements of the major reactive nitrogen species $(NO_y)_i$ (NO_x, peroxyacyl nitrates, HNO_3, and particulate nitrate (NO_3^-)), total reactive nitrogen (NO_y), volatile organic compounds, OH and HO_2, and organic aerosol were made near the urban center of Tokyo in different seasons of 2003–2004 to study the processes involving oxidized forms of reactive nitrogen and O_3. Generally, NO_x constituted the dominant fraction of NO_y throughout the seasons. The NO_x/NO_y and HNO_3/NO_y ratios were lowest and highest, respectively, in summer, owing to the seasonally high OH concentration. The fraction of NO_y that remained in the atmosphere after emission (R_{NOy}) decreased with the decrease in the NO_x/NO_y ratio in summer and fall. It is likely that the median seasonal-diurnal variations of $O_x = O_3 + NO_2$ were controlled by those of the background O_3 levels, photochemical O_3 formation, and vertical transport. O_x showed large increases during midday under stagnant conditions in mid-August 2004. Their in situ production rates calculated by a box model were too slow to explain the observed increases. The high O_x was likely due to the accumulation of O_x from previous days in the upper part of the boundary layer (BL) followed by transport down to near the surface by mixing after sunrise. Considering the tight correlation between O_x and secondary organic aerosol (SOA), it is likely that SOA also accumulated during the course of sea-land breeze circulation in the BL.

Citation: Kondo, Y., et al. (2008), Formation and transport of oxidized reactive nitrogen, ozone, and secondary organic aerosol in Tokyo, *J. Geophys. Res.*, *113*, D21310, doi:10.1029/2008JD010134.

1. Introduction

[2] Large amounts of reactive gases, in particular NO_x and volatile organic carbons (VOCs), are emitted from urban areas. Megacities, including the Tokyo Metropolitan Area (TMA) are very large concentrated sources of these species, affecting local, regional, and global O_3 and aerosol levels [*Guttikunda et al.*, 2005; *Ramanathan et al.*, 2007]. In urban areas, O_3 is mainly produced by reactions between NO and peroxy radicals generated from oxidation of carbon monoxide (CO) and VOCs initiated by reaction with OH [e.g., *Thornton et al.*, 2002; *Kleinman et al.*, 2005]. The oxidation of NO_x can lead to the formation of nitric acid (HNO_3), nitrate aerosol (NO_3^-), and peroxyacyl nitrates (PANs). Oxidation of VOCs also leads to the formation of secondary organic aerosol (SOA) [e.g., *de Gouw et al.*, 2005; *Sullivan et al.*, 2006; *Takegawa et al.*, 2006b], although the chemical species contributing to the O_3 and SOA formation are different [e.g., *Odum et al.*, 1997; *Hoffmann et al.*, 1997; *Griffin et al.*, 1999]. SOA generally constitutes the major fraction of fine-mode aerosol mass concentration. Reactive nitrogen, O_3, and SOA play important roles in the atmospheric environment, including acid deposition, effects on human health, visibility, and climate. In order to assess the impacts of NO_x and VOCs emitted from local sources on surrounding areas, we need to understand quantitatively the key processes involved in their oxidation and the fate of the oxidized species near the source regions.

[3] The abundance of NO_x is controlled by its emission, oxidation, and transport. During daytime, NO_x is oxidized to HNO_3 via oxidation of nitrogen dioxide (NO_2) by the hydroxyl radical (OH):

$$\text{(R1)} \qquad NO_2 + OH + M \rightarrow HNO_3 + M,$$

[1] Research Center for Advanced Science and Technology, University of Tokyo, Tokyo, Japan.
[2] Asian Environment Research Group, National Institute for Environmental Studies, Ibaraki, Japan.
[3] Frontier Research Center for Global Change, Japan Agency for Marine-Earth Science and Technology, Kanagawa, Japan.
[4] Now at Institute of Low Temperature Science, Hokkaido University, Sapporo, Japan.
[5] National Institute of Water and Atmospheric Research, Lauder, New Zealand.
[6] Department of Chemistry, University of California, Irvine, California, USA.
[7] Faculty of Marine Technology, Tokyo University of Marine Science and Technology, Tokyo, Japan.
[8] Department of Earth and Planetary Science, Graduate School of Science, University of Tokyo, Tokyo, Japan.

0148-0227/08/2008JD010134

where M represents a third body (usually N_2 or O_2). During the nighttime, HNO_3 is formed via oxidation of NO_2 followed by hydrolysis of N_2O_5 in aqueous-phase H_2O (H_2O (aq)) [e.g., *Tie et al.*, 2003; *Takegawa et al.*, 2004]:

$$(R2) \qquad N_2O_5 + H_2O(aq) \rightarrow 2HNO_3.$$

HNO_3 reacts with gas-phase NH_3 to form ammonium nitrate (NH_4NO_3) aerosol:

$$(R3) \quad HNO_3(g) + NH_3(g) \rightleftharpoons NO_3^-(aerosol) + NH_4^+(aerosol).$$

[4] HNO_3 and NO_3^- are lost through wet and dry deposition. The deposition velocity of NO_3^- is an order of magnitude smaller than that of HNO_3 [e.g., *Morino et al.*, 2006, and references therein].

[5] NO_2 is also oxidized by peroxyacyl radicals ($RC(O)O_2$) to form PANs ($RC(O)O_2NO_2$ = peroxyacetyl nitrate (PAN) + peroxypropionyl nitrate (PPN) + peroxy-n-butyryl nitrate (PnBN) + peroxy-i-butyryl nitrate (PiBN) + peroxyacrylic nitric anhydride (APAN) + peroxymethacryloyl nitrate (MPAN)) [e.g., *Tanimoto et al.*, 1999; *Tanimoto and Akimoto*, 2001; *Roberts et al.*, 2001]:

$$(R4) \qquad RC(O)O_2 + NO_2 \rightleftharpoons RC(O)O_2NO_2.$$

$RC(O)O_2$ is produced by oxidation of VOCs by OH. Acyl radicals formed from aldehydes and alcohols quickly add oxygen to form peroxyacyl radicals. PANs are thermally unstable and decompose back to NO_2 quickly at high temperatures. In addition, alkyl nitrates ($RONO_2$) have been observed to constitute a significant portion of oxidized reactive nitrogen [*Day et al.*, 2003].

[6] Chemical processes of reactive nitrogen inside megacities control fluxes of NO_x and oxidized reactive nitrogen to surrounding regions. A number of studies have been made to understand oxidation processes of NO_x and the resulting partitioning of total reactive nitrogen, NO_y (=NO + NO_2 + PANs + HNO_3 + HONO + HO_2NO_2 + NO_3 + N_2O_5 + organic nitrate + NO_3^-), in urban and suburban air through field observations at various locations, mainly over the U.S. and Europe [e.g., *Fahey et al.*, 1986; *Singh et al.*, 1986; *Parrish et al.*, 1993, 1998, 2002; *O'Brien et al.*, 1997; *Ridley et al.*, 1998; *Neuman et al.*, 2002; *Day et al.*, 2003]. These observations identified NO_x, HNO_3, and PANs to be dominant components of NO_y, although their fractions showed large temporal and spatial variations. However, quantitative understanding of the reactions involving these species is still limited partly because of the difficulty in deploying a suite of instruments for accurate and time-resolved measurements of relevant parameters throughout the seasons. On the other hand, the rate-limiting reactions for O_3 formation are

$$(R5) \qquad HO_2 + NO \rightarrow OH + NO_2,$$

$$(R6) \qquad RO_2 + NO \rightarrow RO + NO_2.$$

[7] The processes of oxidation of NO_x and VOCs via OH are closely coupled with the O_3 formation processes via formation of HO_2 and RO_2, as can be seen from reactions (R1)–(R6) [e.g., *Kanaya et al.*, 2007, 2008]. Therefore, it is useful to elucidate the relationships of the reactive nitrogen, HO_x (OH and HO_2) radicals, and O_3 for an improved understanding of O_3 formation, especially near urban areas, where reactions leading to its formation are active. In addition, SOA have been observed to correlate well with O_3 in summertime in the TMA [*Takegawa et al.*, 2006a; *Miyakawa et al.*, 2008]. O_3, together with OH and NO_3, oxidize VOCs, initiating a number of chemical and physical processes leading to SOA formation [e.g., *Kalberer et al.*, 2000]. Therefore, SOA-O_3 correlations should also be useful in understanding the chemistry of these species.

[8] In addition to the chemical processes, the levels of reactive nitrogen and O_3 are subject to transport processes. In the TMA, it has been suggested that accumulation of formed O_3 in the boundary layer (BL) plays an important role in elevating surface O_3 levels under stagnant conditions in summer [*Wakamatsu et al.*, 1983, 1996, 1999]. However, these studies are limited to O_3 variations. Simultaneous measurements of oxidized reactive nitrogen and SOA will give us further insights on transport processes of the oxidized species in this area.

[9] Intensive measurements of reactive nitrogen, together with other precursors of O_3 and PM_1 aerosol (aerosol with diameters smaller than 1 μm) chemical composition were made for the first time in Tokyo, Japan, in 2003–2004, as a part of the series of the Integrated Measurement Program for Aerosol and Oxidant Chemistry in Tokyo (IMPACT) campaigns, which were conducted within the framework of the International Global Atmospheric Chemistry Project (IGAC), Mega-Cities: Asia. Using these data, we investigate the seasonal and diurnal variations of reactive nitrogen species, especially in relation to HO_x radicals and O_3 near the urban center of Tokyo. The relationship between O_3 and SOA in summer is also discussed.

2. Observations

2.1. Location and NO_x Sources

[10] NO_y, individual NO_y compounds, and PM_1 aerosol were measured near the urban center of Tokyo during the periods of 24 July to 13 August and 1–15 October in 2003 and 20 January to 6 February, 16 June to 7 July, and 26 July to 14 August in 2004. Air samplings were made about 20 m above ground level from a building on the Research Center of Advanced Science and Technology (RCAST) campus of the University of Tokyo (Komaba; 35.66°N, 139.66°E) in Japan. RCAST is located 57 m above sea level and about 2 km from major roads or highways, near the southeastern edge of the Kanto Plain, about 20 km from Tokyo Bay [*Kondo et al.*, 2006; *Takegawa et al.*, 2006a; *Morino et al.*, 2006], as shown in Figure 1.

[11] Figure 1 also shows the distribution of NO_x emissions in the TMA estimated by *Kannari et al.* [2004]. The TMA is defined as the area over seven prefectures labeled in Figure 1. The relative contributions of different sources are summarized in Table 1. Motor vehicles are estimated to be the dominant contribution (55%) to NO_x emissions in the TMA. Emissions from diesel vehicles are estimated to be particularly important to NO_x emissions in the TMA (38%). RCAST is located within a high-NO_x emission area. How-

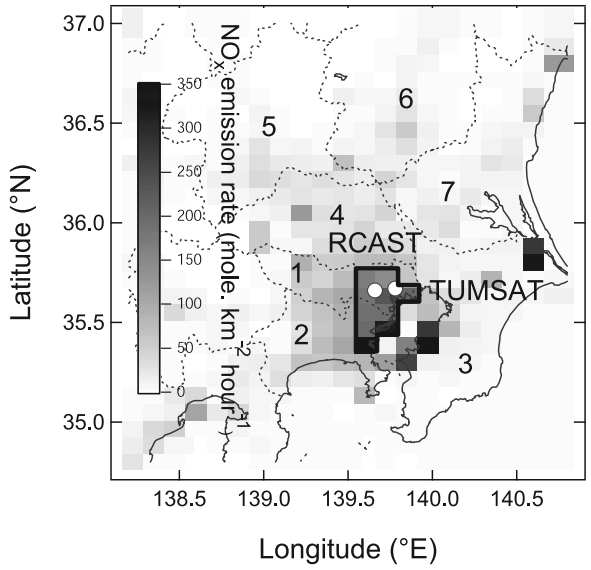

Figure 1. Map of the NO_x emission rate over the Kanto Plain. The observational sites (Research Center of Advanced Science and Technology (RCAST) and Tokyo University of Marine Science and Technology (TUMSAT)) are shown as open circles. The high-NO_x emission areas are depicted by thick lines (approximate urban boundary).

ever, the measurements presented here were not significantly influenced by emissions from highly localized sources, as discussed in section 3.1.

2.2. Instrumentation

[12] Table 2 summarizes the measurements used for the present study, including accuracies, precisions, and time resolutions. The key measurements at RCAST are described in brief below. NO, NO_2, and NO_y were measured using a NO-O_3 chemiluminescence detector [*Kondo et al.*, 1997; *Nakamura et al.*, 2003; *Miyazaki et al.*, 2005]. The ambient air was sampled through a 2-m-long perfluoroalkoxy (PFA) hose with a 4.6-cm inner diameter (ID) at a flow rate of 1200 standard liter per minute (slm). From the center of the unheated hose, a small portion of the ambient air was drawn up into the NO, NO_2, and NO_y instrument by way of a 6.35-mm-outer-diameter (OD) PFA tube (1 m long) heated to 35°C. NO_y was catalytically converted to NO on the surface of a gold tube heated to 300°C. The conversion efficiency of particulate NH_4NO_3 (boiling point 210°C) was measured to be 91 ± 9%, while the conversion efficiencies for KNO_3, $NaNO_3$, and $Ca(NO_3)_2$ were 1, 2, and 3% respectively [*Miyazaki et al.*, 2005]. The overall collection efficiency of NH_4NO_3 should be close to 1, because of high flow in the PFA hose, heated PFA tube, and high conversion efficiency. On the other hand, $NaNO_3$ in sea salt is excluded from NO_y because of the conversion efficiency close to zero. NO_2 was converted to NO by a photolytic converter (Droplet Measurement Technologies, Inc., USA) with a conversion efficiency of about 30–40%. Systematic errors of the measurements of NO, NO_2, and NO_y were 10, 16, and 12%, respectively. The random errors of the NO, NO_2, and NO_y measurements with 1-min time averaging were ±4 parts per trillion by volume (pptv), ±9 pptv, and ±68 pptv, respectively, for their typical ambient mixing ratios.

[13] HNO_3 was measured by a chemical ionization mass spectrometer (CIMS) using the selective ion-molecule reaction of SiF_5^- with HNO_3 [*Kita et al.*, 2006; *Morino et al.*, 2006]. We used the same PFA hose, as that used for the NO_y measurements, for ambient air sampling. The detection limit for a 10-s integration was 19 pptv, and the overall accuracy was about 9% at an HNO_3 mixing ratio of 1 part per billion by volume (ppbv). Interference of particulate NO_3^- to the HNO_3 measurements was negligible [*Kita et al.*, 2006].

[14] Particulate NO_3^-, predominantly in the form of NH_4NO_3, was measured using an Aerodyne Aerosol Mass Spectrometer (AMS) with a time resolution of 10 min [*Takegawa et al.*, 2005; *Morino et al.*, 2006]. Organic aerosol (OA) was also measured by AMS [*Takegawa et al.*, 2005]. The sample line from the inlet to the AMS consisted of a $PM_{2.5}$ (2.5 μm) cyclone and a 1-mm-inner-diameter stainless steel tube (6 m long). The AMS measurements were compared extensively with a particle-into-liquid sampler combined with an ion chromatography analyzer (inorganic components) and a Sunset Laboratory semicontinuous thermal-optical carbon analyzer (organics). The detection limits of nitrate and OA were 0.02 and 0.3 μg m^{-3}, respectively [*Takegawa et al.*, 2005]. The actual size cut of the AMS was determined to be nearly PM_1 (1 μm) by the more restrictive transmission characteristics of the aerodynamic lens.

[15] Each species of PANs (=PAN + PPN + PnBN + PiBN + APAN + MPAN) was measured every 15 min using a gas chromatograph with a negative ion chemical ionization mass spectrometer [*Tanimoto et al.*, 1999, 2002]. The detection limit for PAN, a dominant species of PANs, was 15 pptv with an overall measurement uncertainty of 20%. VOCs, including alkyl nitrates and nonmethane hydrocarbons (NMHCs) ($RONO_2$; C_1-C_5) were measured using whole air sampling followed by laboratory analysis using gas chromatography [*Blake et al.*, 2003a, 2003b; *Simpson et al.*, 2003, and references therein]. Although the sampling interval was 2–6 h, the actual integration time was 5–10 s for each sample. The whole air sample data were merged with the other data without further averaging or smoothing. The $RONO_2$ data were available only for the summer period. The temporal variations of C_2-C_7 VOCs are shown by *Shirai et al.* [2007].

[16] CO was measured using a nondispersive infrared absorption (NDIR) instrument (Model-48, Thermo Environmental Instruments (TEI), USA). The overall precision and accuracy of the 1-min CO data were estimated to be 4 ppbv and 20 ppbv, respectively, at a CO mixing ratio of 400 ppbv [*Kondo et al.*, 2006]. O_3 was measured using an ultraviolet

Table 1. NO_x Emissions in Tokyo and the TMA

	Tokyo[a] (Gg/a)	TMA[a] (Gg/a)
Total	153 (100)	337 (100)
Energy industries	35 (23)	43 (13)
Manufacturing industries and construction	25 (16)	66 (20)
Transport (total)	74 (48)	187 (55)
Transport (gasoline)	14 (9)	35 (11)
Transport (diesel)	46 (30)	129 (38)
Transport (others)	14 (9)	23 (6)
Other sectors (commercial, etc.)	13 (8)	26 (8)
Waste incineration	7 (4)	15 (5)

[a]Relative contribution in percent is given in parentheses.

Table 2. Systematic and Random Errors in the Mixing Ratios of Measured Trace Gases, Aerosols, and Meteorological Parameters

Species	Technique	Accuracy (%)	1σ Precision	Time Resolution	Integration Time	Reference
NO	chemiluminescence (CL)	10 (at 2 ppbv)	4 pptv (at 2 ppbv)	1 min	10 s	*Kondo et al.* [1997]
NO_2	CL with photolysis converter	16 (at 13 ppbv)	9 pptv (at 13 ppbv)	1 min	10 s	*Nakamura et al.* [2003]
NO_y	CL with heated gold converter	12 (at 21 ppbv)	68 pptv (at 21 ppbv)	1 min	10 s	*Kondo et al.* [1997]
HNO_3	chemical ionization mass spectrometer	9 (at 1 ppbv) 19 (at 50 pptv)	23 pptv	1 min	1 min	*Kita et al.* [2006]
PANs	gas chromatography with negative ion chemical ionization mass spectrometer	20 for PAN 25 for PPN	LOD: 15 pptv for PAN and 26 pptv for PPN	15 min	1 min	*Tanimoto et al.* [1999]
NO_3^-, OA	aerosol mass spectrometer	26 25	0.01 μgm^{-3} (NO_3^-), 0.1 μgm^{-3} (OA)	10 min	10 min	*Takegawa et al.* [2005] and *Kondo et al.* [2007]
Alkyl nitrates	air sampling and gas chromatography with electron capture detection			2–6 h	5–10 s	*Blake et al.* [2003a, 2003b] and *Simpson et al.* [2003]
OH	laser-induced fluorescence	20	LOD: 5.2×10^5 cm^{-3} for daytime and 1.3×10^5 cm^{-3} for nighttime	10 min		*Kanaya et al.* [2001a, 2001b, 2007]
HCHO, CH_3CHO	proton transfer reaction mass spectrometry		0.81 ppbv for HCHO and 0.12 ppbv for CH_3CHO	10 s 1 s	1 min	*Kanaya et al.* [2007]
HONO	diffusion scrubber/ion chromatography		20 pptv	30 min	30 min	*Kanaya et al.* [2007]
CO	IR absorption	5 (at 400 ppbv)	4 ppbv (at 400 ppbv)	1 min	1 min	*Kondo et al.* [2006]
O_3	UV absorption	5	1 ppbv	1 min	1 min	
$J(O^1D)$, $J(NO_2)$	spectroradiometer	20		2 min		*McKenzie et al.* [2002]
Wind, temperature, and RH				10 min		*Kondo et al.* [2006]

(UV) absorption instrument (Model 1101, Dylec, Japan). The instrument was calibrated with a standard O_3 generator (Thermo Electron Inc., Model 49PS, USA). The precision was 0.3 ppbv, defined as a standard deviation (1σ) of the difference between the 1-min values of the O_3 instrument and those measured by the calibration instrument at O_3 concentrations of about 50 ppbv. The accuracy of the O_3 data was estimated to be about 5%, equal to the accuracy of the standard O_3 generator. This O_3 generator is traceable to a National Institute of Standards and Technology (NIST) standard.

[17] OH and HO_2 were measured using a laser-induced fluorescence (LIF) technique [*Kanaya et al.*, 2001a, 2001b, 2007]. The overall uncertainties in OH and HO_2 measurements were estimated to be ±24% for OH and ±26% for HO_2 (1σ). The detection limit for the 10-min data was 1.3×10^5 cm^{-3} for nighttime and 5.2×10^5 cm^{-3} for daytime. Formaldehyde (HCHO) and acetaldehyde (CH_3CHO) were measured by a proton-transfer-reaction mass spectrometry (PTR-MS) technique only during the winter campaign [*Kanaya et al.*, 2007]. The signals were integrated for 10 s and 1 s for HCHO and CH_3CHO, respectively. HONO was measured using diffusion scrubber/ion chromatography, also in winter.

[18] Photolysis frequencies of O_3 ($J(O^1D)$) and NO_2 ($J(NO_2)$) were derived from actinic flux measurements from a spectroradiometer that was developed by New Zealand's National Institute of Water and Atmospheric Research (NIWA) [*McKenzie et al.*, 2002]. The instrument scanned the spectral region between 285 and 450 nm with a sampling interval of 0.2 nm and a spectral resolution of approximately 0.65 nm. Radiometric calibration was made with respect to the NIST standard, with a total uncertainty of approximately ±6%. Additional uncertainties arose from uncertainties in the absorption cross sections and quantum yields that were used to convert these actinic fluxes to photolysis rates. For $J(O^1D)$ and $J(NO_2)$ we used absorption cross sections by *Molina and Molina* [1986] and *Harder et al.* [1997], respectively, and quantum yields recommended by JPL [*DeMore et al.*, 1997]. The instrument measures only the downwelling component of the actinic flux. For UV observations near the surface, the lack of the upwelling component results in only a small error because of the low surface albedo at these wavelengths. Local horizon obscurations limited the instrument field of view to approximately 90% of the full hemisphere, resulting in an underestimation of approximately 10% in the diffuse component of the radiation field. The direct sun was sometimes blocked in the morning up to solar elevations of 20°. However, at those solar elevations, the actinic flux is dominated by the diffuse skylight component, and the overall reduction in actinic fluxes due to horizon obscurations was generally less than 10%. Taking all of the above uncertainties into consideration, we estimate the overall uncertainty in the derived photolysis rates to be ±20%. Most of the data described above (gases, aerosols, and actinic flux) were merged into time intervals of 10 min for the present analysis.

[19] In addition to the measurements at RCAST, concentrations of inorganic aerosol were measured by collecting aerosol particles on quartz fiber filters using a high-volume filter sampler (Model 130, Kimoto, Osaka, Japan), followed by analysis using an ion chromatography analyzer at the

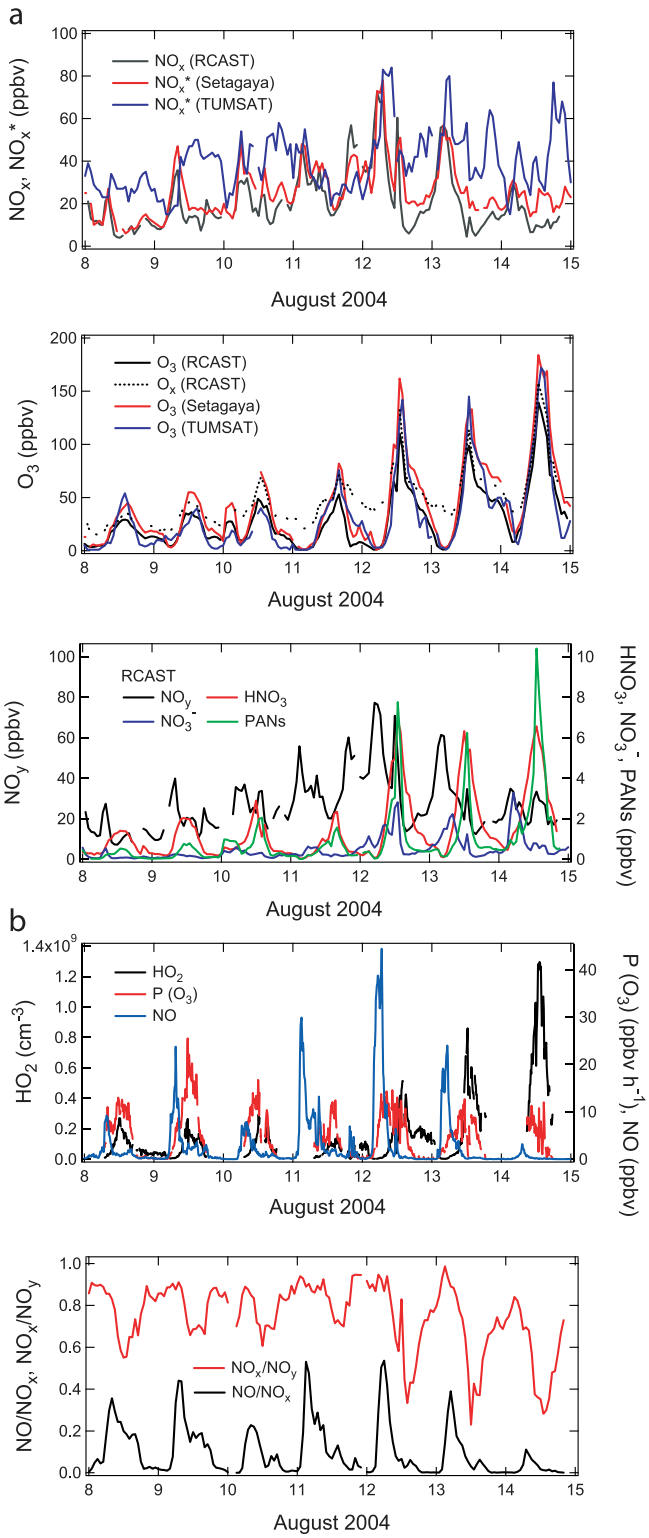

Figure 2. (a) Temporal variations of the 1-h average values of NO_x, NO_x^*, O_3, $O_x = O_3 + NO_2$, NO_y, HNO_3, NO_3^-, and peroxyacyl nitrates (PANs) for 1 week (8–14 August) in the summer of 2004. (b) Temporal variations of the 10-min-averaged values of NO, HO_2, and $P(O_3)$ and 1-h-averaged NO/NO_x and NO_x/NO_y ratios for 1 week (8–14 August) in the summer of 2004.

Etchujima campus (35.66°N, 139.80°E) of the Tokyo University of Marine Science and Technology (TUMSAT). TUMSAT is located 10 km east of RCAST (Figure 1). The sampling of aerosol particles was made in two size ranges using an impactor with diameters larger than 2 μm (coarse mode) and smaller than 2 μm (PM_2) [*Murayama et al.*, 1999].

2.3. Box Model

[20] In this work we used a photochemical box model to calculate RO_2 (organic peroxy) radical concentrations to derive ozone formation ($F(O_3)$), destruction ($D(O_3)$), and net formation ($P(O_3)$) rates. The O_3 formation processes include reactions (R5) and (R6). $F(O_3)$ and $D(O_3)$ are expressed as

$$F(O_3) = \left(k_{HO2+NO}[HO_2] + \Sigma\, k_{RO2+NO}\varphi[RO_2]\right)[NO], \quad (1)$$

where [ ] denotes the number density of the indicated species, k is the reaction rate coefficient of the corresponding reaction indicated by the suffix, and φ is the yield of NO_2 from reaction (R6):

$$D(O_3) = k_{O1D+H2O}[O^1D][H_2O] + (k_{OH+O3}[OH] + k_{HO2+O3}[HO_2] + \Sigma\, k_{olefin+O3}[olefin])[O_3] + k_{OH+NO2}[NO_2][OH], \quad (2)$$

$$P(O_3) = F(O_3) - D(O_3). \quad (3)$$

Observed HO_2 concentrations and model-calculated RO_2 were used in equations (1) and (2). Briefly, the box model takes into account the Regional Atmospheric Chemistry Mechanism (RACM) [*Stockwell et al.*, 1997] with updated kinetic parameters. The heterogeneous loss of HO_2 is not taken into account in the standard runs. For constraining the model, we used the observed concentrations and parameters (O_3, CO, H_2O, SO_2, NO, NO_2, CH_4, NMHCs, PANs, temperature, ambient pressure, and J values) in the analysis of the winter and summer data. In total, 54 NMHCs were taken into account in the 11 model categories, as described by *Kanaya et al.* [2007]. For winter, the measured concentrations of HONO, HCHO, and CH_3CHO were also used to constrain the model. Summertime concentrations of HONO were calculated by the model. HCHO and CH_3CHO concentrations estimated empirically from CO and (O_3 + NO_2) concentrations were used for the summer period. All of the other oxygenated species were calculated in the model, with an assumption that dilution occurred with a time constant of 6 h to represent horizontal advection of air masses influenced by urban emissions.

[21] We compared the model-calculated HO_2 values with the observed values to check the reliability of the calculated RO_2 used in calculating $P(O_3)$. For winter, the model-calculated OH and HO_2 levels during the daytime agreed better with observations when the concentrations of internal olefin (OLI in RACM) and reactive alkanes (HC8) were increased by factors of 3 and 5, respectively (run 2), above the standard-run hydrocarbon levels. Therefore, the calculated RO_2 from run 2 and the observed HO_2 were used to calculate $P(O_3)$.

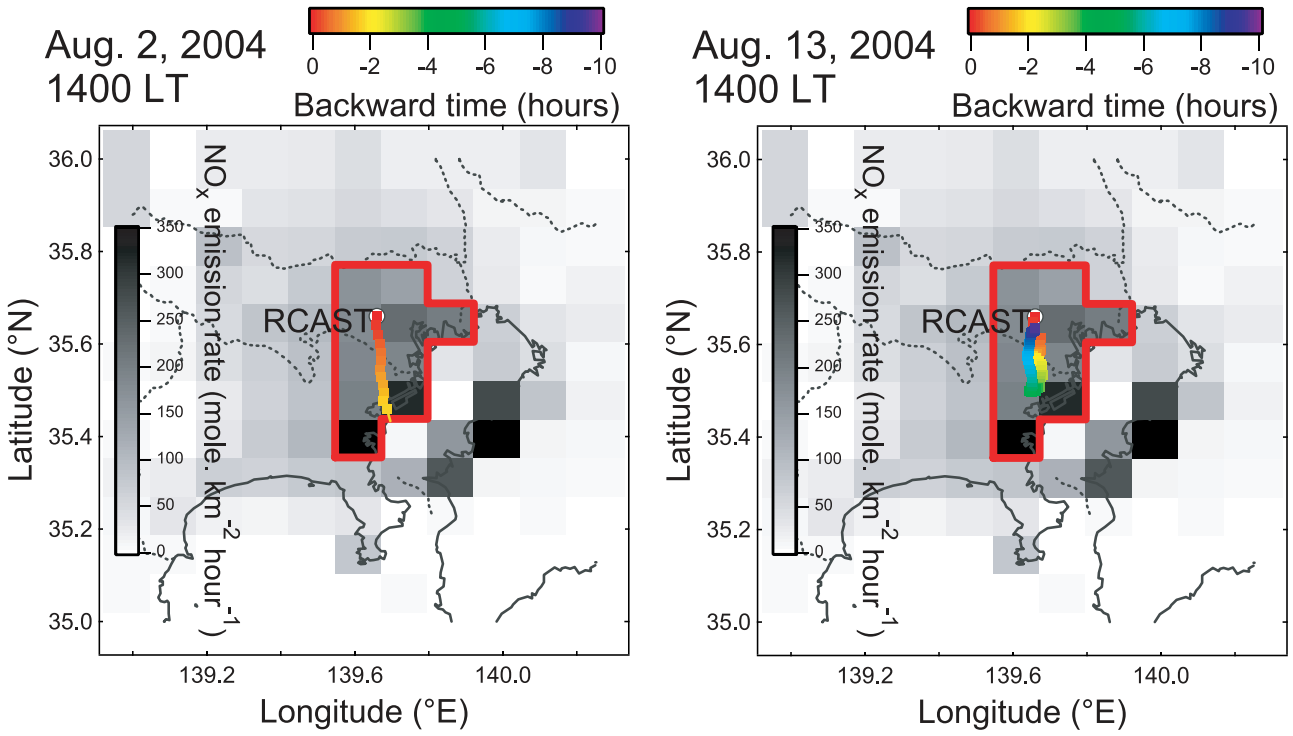

Figure 3. Trajectories of air masses sampled at RCAST at 1400 LT on 2 and 13 August 2004. The high-NO_x emission areas (urban boundary) are marked in red. The locations of air masses are color-coded according to the residence time in the high-NO_x emission areas (blue to red).

[22] For summer, increased OLI and HC8 concentrations lead to a significant overestimation of HO_2 by the model. Therefore the calculated RO_2 from the standard run and the observed HO_2 were used for the $P(O_3)$ calculations, although the effect of using the different levels of RO_2 on $P(O_3)$ was not significant. More detailed descriptions of the model and the comparisons between calculated and observed OH and HO_2 radical concentrations have been given by *Kanaya et al.* [2007].

[23] The same box model was used to simulate temporal variations of PAN in summer, with slightly different settings. In this case, the constraint on PAN concentrations was removed and its concentrations were predicted considering photochemical processes included in RACM, a deposition term with a velocity of 0.2 cm s^{-1}, and a dilution term with a time constant of 6 h. The BL height was assumed to be 1000 m in the daytime and 100 m in the nighttime to calculate the loss rate owing to surface deposition. The model-calculated PAN concentrations are compared with those observed in section 6.1.

3. Temporal Variations of Reactive Nitrogen and Oxidants

3.1. Spatial Uniformity of the Observational Data

[24] Figure 2a shows a 1-h resolution time series of NO_x, O_3, and O_x measured at RCAST and of NO_x^* and O_3 at routine monitoring stations of the Atmospheric Environmental Regional Observation System (AEROS) (http://soramame.taiki.go.jp/) at Setagaya (5 km southwest of RCAST) and at a site very close to TUMSAT during the summertime period to illustrate the spatial uniformity of these species near the urban center of Tokyo. Here O_x represents oxidants O_3 + NO_2, taking into account conversion of O_3 to NO_2 (O_3-NO titration). The nighttime decrease of O_x was significantly smaller than that of O_3, because O_x is better conserved than O_3. Figure 2a also shows time series of HNO_3, NO_3^-, PANs, and NO_y. NO_x^* represents reactive nitrogen measured using molybdenum converters with particulate filters mounted upstream of chemiluminescence NO detectors. The conversion efficiencies of molybdenum converter for NO_2, HNO_3, and PAN were observed to be close to those for gold catalytic converter [*Fehsenfeld et al.*, 1987]. However, the unheated filter and metal plumbing parts removed HNO_3 and particulate nitrate, although the removal efficiencies were not quantified. The NO_x^* levels measured at RCAST during a different period were found to be between the NO_x and NO_y levels (not shown). It is likely that NO_x^* represents NO_x + organic nitrates. Temporal variations of NO_x and NO_x^* measured at RCAST and Setagaya were similar, indicating that the air masses observed at RCAST were not significantly affected by localized sources. The differences in the NO_x^* variations between Setagaya and TUMSAT were larger than those between RCAST and Setagaya, although the average NO_x^* levels were similar. It is likely that the larger differences between Setagaya and TUMSAT reflect the relatively short lifetime of NO_x (about 8 h) and differences in the accumulated amounts of NO_x along trajectories of air masses sampled at these sites, as discussed in detail in Appendix A. The temporal variations of the O_3 concentration at the three sites were very similar. These features of NO_x and O_3 were basically the same for other seasons, suggesting their spatial

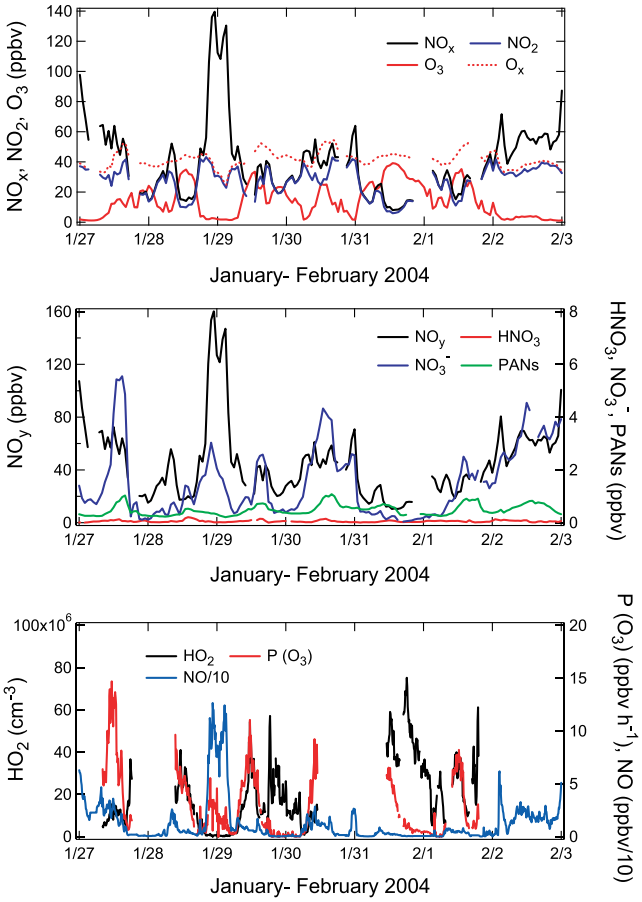

Figure 4. Temporal variations of the 1-h-averaged values of O_3, NO_2, NO_x, O_x, NO_y, HNO_3, NO_3^-, PANs, O_3, NO, HO_2, and $P(O_3)$ for 1 week (27 January to 2 February) in the winter of 2004.

uniformity near the urban center of Tokyo throughout the seasons.

3.2. Reactive Nitrogen and $P(O_3)$

[25] Figure 2b shows time series of NO, HO_2, $P(O_3)$, and NO_x/NO_y and NO/NO_x ratios at RCAST during the latter part of the summertime period. The whole summertime observation period of 31 July to 14 August in 2004 was classified into two phases according to meteorological conditions, as discussed in previous studies [*Takegawa et al.*, 2006b; *Miyakawa et al.*, 2008]. Detailed meteorological analyses in relation to concentrations of VOCs and CO have been given by *Shirai et al.* [2007]. Phase 1 is from 31 July to 9 August, when persistent southerly wind flows (wind speed > 2 m s^{-1}) were dominant, as shown in Figure 3 of *Shirai et al.* [2007]. The concentrations of O_3 were relatively low because clean maritime air was transported from the Tokyo Bay to RCAST.

[26] Phase 2 is from 10 August to 15 August, when sea-land breeze circulation was dominant. Generally the wind speed was weaker than during phase 1, and the wind was southerly or southeasterly in the afternoon and mostly northerly or northeasterly in the night and early morning. The diurnal change in the wind direction over the TMA is shown in Figure 4 of *Shirai et al.* [2007]. During this phase, the concentrations of O_3, HNO_3, and PANs showed large increases in the daytime, especially during the period of 12–14 August. SOA also showed simultaneous increases during this period [*Kondo et al.*, 2007; *Miyakawa et al.*, 2008].

[27] The difference in the circulation between phases 1 and 2 is clearly reflected in the trajectories of air masses sampled at RCAST at 1400 LT on 2 and 13 August, as shown in Figure 3. The backward trajectories were calculated using the wind data obtained at RCAST. The high-emission areas in the study region are marked in red. A more detailed description of the trajectory calculation is given in Appendix A. The air originating from RCAST at 0400 LT moved southward and returned to the original site at 1400 LT on 13 August. On 2 August, air originating near the coast of the Tokyo Bay reached RCAST in about 2 h.

[28] Figure 4 shows time series of O_3, NO_2, NO_x, O_x, NO_y, HNO_3, NO_3^-, PANs, O_3, NO, HO_2, and $P(O_3)$ at RCAST for the winter period. The nighttime decrease of O_3 was much smaller than that of O_x, similar to summer. In winter, HNO_3 levels were much lower and NO_3^- levels were much higher than in summer as discussed by *Morino et al.* [2006]. PANs showed stable background levels with some daytime increases. However, the level of the daytime enhancements was much lower than that in phase 2 in summer. NO_y and NO_3^- concentrations showed increases with a period of about 3–4 days, lasting for about 2 days. Primary organic aerosol (POA) and SOA showed correlated increases, as shown in Figure 3 of *Kondo et al.* [2007]. Weak wind conditions favored accumulation of all these species. On a larger perspective, the periodic synoptic-scale cyclonic activity typical for this season set these conditions (Y. Morino et al., manuscript in preparation, 2008).

4. Median Diurnal and Seasonal Variations

4.1. $J(O^1D)$, OH, and HO_2

[29] For a statistical analysis of NO_x oxidation and O_3 formation processes, the observed data sets were classified into two categories on the basis of $J(O^1D)$ values. High-$J(O^1D)$ (HJ) days were defined as days when the maximum values of $J(O^1D)$ within the day exceeded a threshold value, which was determined as half of the maximum value of $J(O^1D)$ in each season. The rest of the data were classified as low-$J(O^1D)$ (LJ) days. The threshold values and the numbers of HJ and LJ days are summarized in Table 3. The HJ and LJ days generally represent sunny and cloudy days, respectively. Figure 5 shows the diurnal variations of the median $J(O^1D)$ values on HJ and LJ days in the three seasons and the median OH and HO_2 concentrations on HJ days in two seasons. $J(O^1D)$ was a good indicator of

Table 3. Number of High- and Low-$J(O^1D)$ Days

	Maximum (Threshold) Values of $J(O^1D)$[a]	Number of High-$J(O^1D)$ Days	Number of Low-$J(O^1D)$ Days
Summer 2003	36 (18) × 10^{-6}	18	2
Fall 2003	22 (11) × 10^{-6}	11	2
Winter 2004	13 (7) × 10^{-6}	16	2
Summer 2004	39 (20) × 10^{-6}	19	0

[a]Threshold values were defined as about half of the maximum values of $J(O^1D)$ for each season and are given in parentheses.

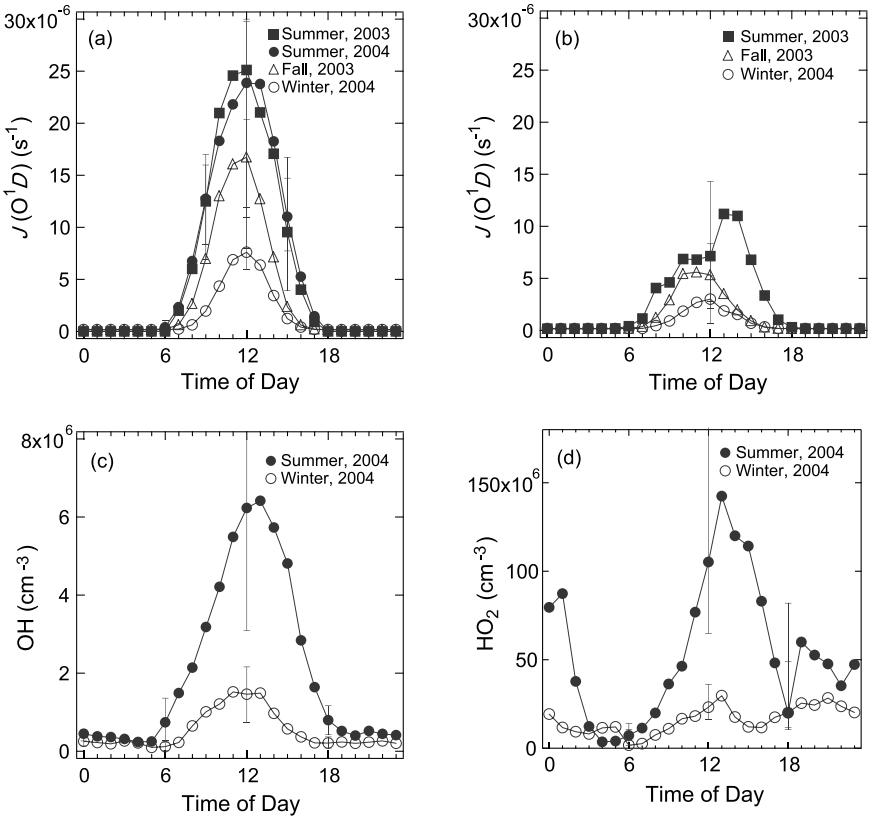

Figure 5. Diurnal variations of the median values of $J(O^1D)$ on (a) high-$J(O^1D)$ (HJ) days in summer (closed squares), fall (open triangles), and winter (open circles) and (b) low-$J(O^1D)$ (LJ) days in summer (closed squares), fall (open triangles), and winter (open circles). (c) The OH concentration on HJ days in summer and winter. (d) The HO_2 concentration on HJ days in summer and winter. Bars represent 1σ values.

photochemical activity, judging from the correspondence between the $J(O^1D)$ values and the OH concentrations. On HJ days between 1000 and 1500 local time (LT) the daytime $J(O^1D)$ values in winter were about 3–5 times lower than those in summer. The daytime $J(O^1D)$ values for LJ days between 1000 and 1500 LT were about 2–3 times lower than those for HJ days. The number of HJ days was much larger than that of LJ days. In addition, precipitation occurred only on one day both in summer and winter. Therefore, when averaged over all HJ and LJ days, the median and average values of the species discussed in this paper are very close to those for HJ days.

[30] OH and HO_2 reached maximum values during daytime in summer and winter. However, in winter, HO_2 showed high values from late afternoon throughout the nighttime comparable to those during midday. Detailed discussion of the temporal variations of OH and HO_2 has been made by *Kanaya et al.* [2007].

[31] The *e*-folding lifetimes of NO_x oxidation (reaction (R1)) on HJ days were calculated using the observed OH concentrations (Table 4). They are estimated to be 6–10 h and 25–39 h during daytime in summer and winter, respectively. For LJ days, when OH data were not available, the NO_x lifetime was estimated using the OH concentrations calculated by the parameterization method given by *Ehhalt and Rohrer* [2000]. The ratios of [calculated OH]/[observed OH] were 0.98 ± 0.62 in summer and 1.0 ± 0.56 in winter for HJ days between 1000 and 1500 LT, indicating the reliability of the calculated OH. The lifetimes of NO_x for LJ days are estimated to be 6–8 times longer than those for HJ days.

4.2. NO_y and NO_x

[32] Figure 6 shows the diurnal variations of the median values of NO, NO_2, NO_x, NO_y, NO_x/NO_y ratio, O_3, and O_x in three seasons and $P(O_3)$ in two seasons for HJ days. The seasonal and diurnal variations of NO_x are consistent with the column NO_2 measurements derived from the spectroradiometer [*McKenzie et al.*, 2008]. The NO_x/NO_y ratios for LJ days are also shown. These values are summarized in

Table 4. Average Daytime OH Concentrations and the Corresponding NO_x Lifetimes

	1000–1500 LT		0600–1800 LT	
	[OH] (cm^{-3})	Lifetime (hours)	[OH] (cm^{-3})	Lifetime (hours)
Winter 2004 (HJ)	1.2×10^6 (observed)	25	0.77×10^6	39
Winter 2004 (LJ)	0.17×10^6 (calculated)	180	0.095×10^6	320
Summer 2004 (HJ)	5.5×10^6 (observed)	6.3	3.5×10^6	10
Summer 2004 (LJ)	0.96×10^6 (calculated)	35	0.58×10^6	57

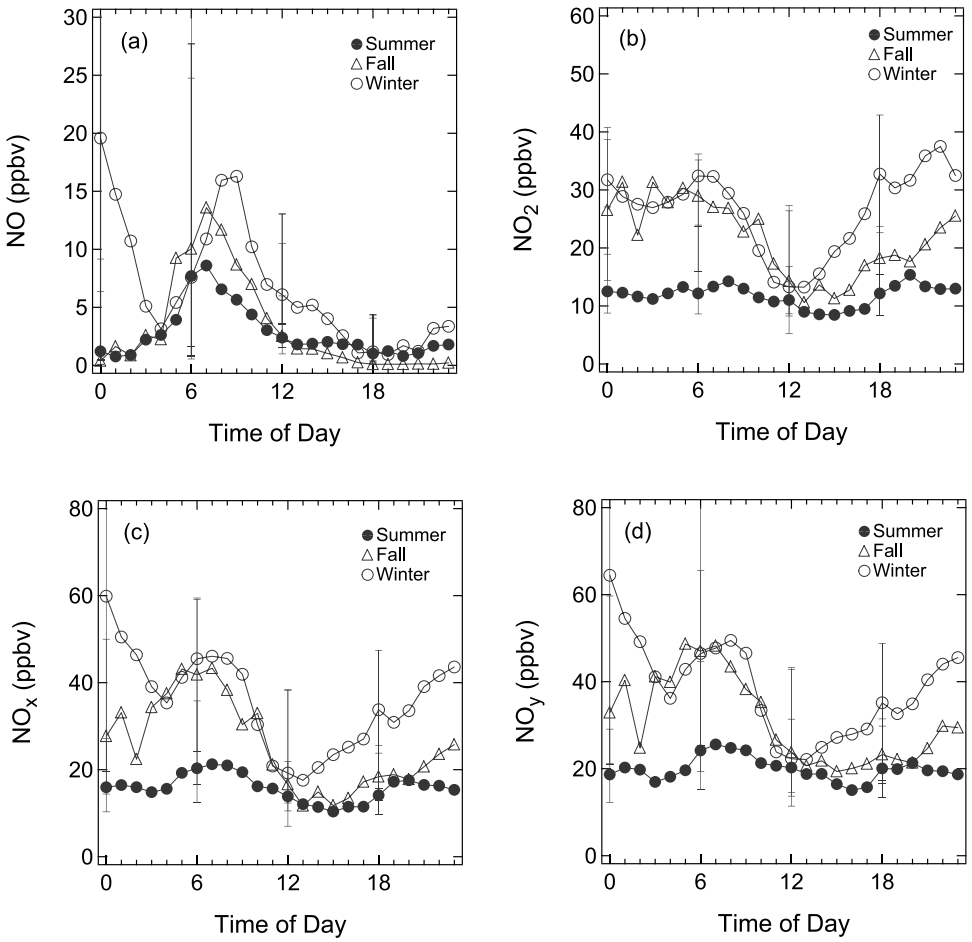

Figure 6. Diurnal variations of median values of (a) NO, (b) NO_2, (c) NO_x, (d) NO_y, (e) NO_x/NO_y ratios, (g) O_3, (h) O_x, and (i) $P(O_3)$ for HJ days in summer (closed circles), fall (open triangles), and winter (open circles). (f) The NO_x/NO_y ratios for LJ days are also shown. Bars represent 1σ values.

Table 5 together with the values of other reactive nitrogen species. The median NO_y (NO_x) concentrations ranged over 20–42 (16–39) ppbv. The NO_y concentrations were generally negatively correlated with wind speed, as has been found for CO and elemental carbon (EC) [*Kondo et al.*, 2006]. The average wind speeds were generally higher during the daytime than during the nighttime, and the frequency of wind speeds exceeding 3 m/s was highest in summer. The BL height also increased after sunrise. Ceilometer observations showed that the top of the BL typically increased from 0.4 km at midnight to 1.5 km at midday. The vertical mixing during the daytime also contributed to the decrease in the concentrations of species emitted from the surface [*Kondo et al.*, 2006; *Morino et al.*, 2006]. Reflecting these dynamic conditions, the NO_x and NO_y concentrations were generally lower during the daytime than during the nighttime, and they were higher in winter than in summer on average.

[33] In addition to these variations caused by the meteorology, the NO_y concentrations peaked in the early morning during summer and fall. In winter, NO_x and NO_y peaked around midnight, in addition to the peak in the early morning, likely owing to the accumulation of these species in the shallow nocturnal wintertime BL. Peaks in EC at the same local times have been ascribed to the emissions from diesel vehicles [*Kondo et al.*, 2006]. It is also very likely that these NO_y peaks were due to enhanced NO_x emissions from heavy-duty diesel vehicles, which are known to emit NO_x and EC much more efficiently than gasoline vehicles [*Miguel et al.*, 1998; *Sawyer et al.*, 2000; *Marr et al.*, 2002].

[34] On HJ days, the median NO_x/NO_y ratios showed significant diurnal variation (Figure 6). The ratios were systematically higher during the nighttime than during the daytime throughout the year. The ratios were lower in summer and fall (0.63–0.89) than those in winter (0.83–0.95). The NO_x/NO_y ratios differed little between summer and fall in spite of the difference in the $J(O^1D)$ values. This is because of the larger removal of NO_y in summer than in fall associated with larger HNO_3/NO_y ratios, as discussed in more detail in section 5.

[35] On LJ days, the median NO_x/NO_y ratios showed little diurnal variation and remained high (mostly above 0.8), irrespective of season. These temporal variations are consistent with the longer lifetimes of NO_x on LJ days.

4.3. HNO_3 and Particulate NO_3^-

[36] The seasonal-diurnal variations of the median values of NO_y species other than NO_x (i.e., HNO_3, NO_3^- (PM_1), total nitrate (TN = HNO_3 + NO_3^-), and PANs) and their

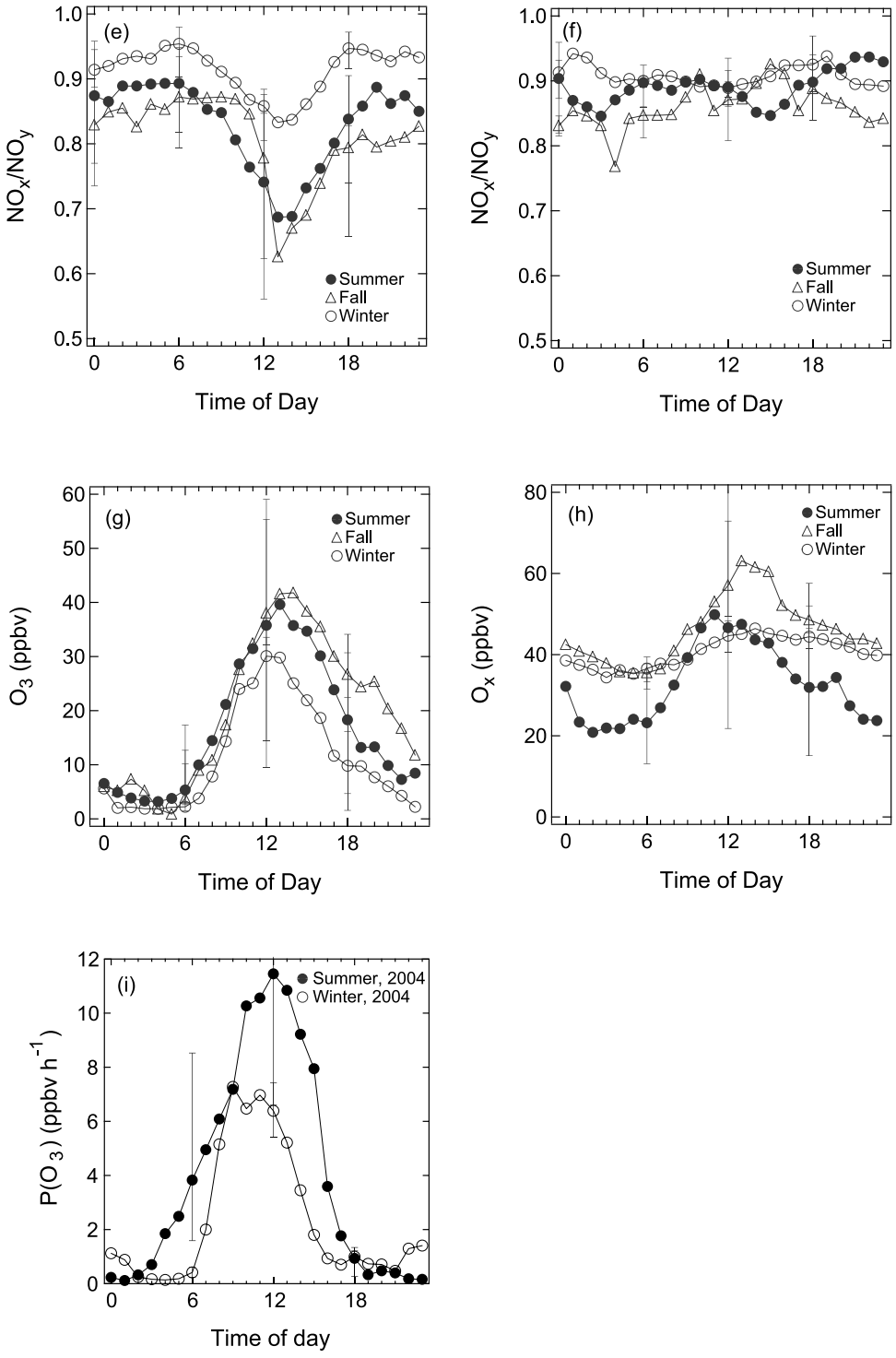

Figure 6. (continued)

ratios to NO_y for HJ days are shown in Figures 7 and 8, respectively. They are also summarized in Table 5.

[37] The temporal variations of HNO_3, NH_3, and NO_3^- were discussed in detail by *Morino et al.* [2006], in terms of chemistry and vertical transport. Here, we discuss the important points relevant to the present analysis. The median HNO_3 concentrations were highest in summer (0.58 ppbv) and lowest in winter (0.06 ppbv). By contrast, the nitrate concentrations were lowest (0.16 ppbv) in summer and highest in winter (1.1 ppbv). The seasonal variation of TN was much reduced compared with each component of TN, that is, HNO_3 and NO_3^-. The seasonal variations of HNO_3 and NO_3^- were due to the seasonal variation of the HNO_3-NO_3^- partitioning. The high (low) temperatures in summer (winter) shifted the HNO_3-NO_3^- partitioning to the gas (aerosol) phase.

[38] In summer and fall, the median HNO_3 concentrations showed a distinct diurnal variation: they started to increase

Table 5. Median and Average Values of NO_x, NO_y, HNO_3, PANs, NO_3^-, Total Nitrate, NO_x/NO_y, HNO_3/NO_y, PANs/NO_y, NO_3^-/NO_y, TN/NO_y, ΔNO_y, TN/NO_z, PANs/NO_z, $\Delta NO_y/NO_z$, CO, O_3, and the Number of Data[a]

	Uncertainty (%)	Summer Median (1σ)	Average	Fall Median (1σ)	Average	Winter Median (1σ)	Average
NO_x	11–12	16 (9.5–26)	19 ± 12	24 (13–49)	30 ± 19	39 (18–68)	45 ± 30
NO_y	12	20 (13–33)	24 ± 14	29 (18–54)	35 ± 20	42 (21–75)	49 ± 33
HNO_3	11–34	0.58 (0.13–2.0)	1.2 ± 1.6	0.17 (0.07–0.49)	0.33 ± 0.45	0.06 (0.02–0.13)	0.08 ± 0.06
PANs	20	0.14 (0.02–0.64)	0.45 ± 1.0	no data		0.43 (0.28–0.68)	0.48 ± 0.22
NO_3^-	26	0.16 (0.05–0.66)	0.37 ± 0.55	0.37 (0.10–1.5)	0.71 ± 0.84	1.1 (0.33–2.8)	1.5 ± 1.4
TN	20–31	0.92 (0.25–2.7)	1.6 ± 1.9	0.63 (0.30–2.0)	1.0 ± 0.97	1.2 (0.38–2.8)	1.6 ± 1.4
NO_x/NO_y	16–18	0.84 (0.69–0.92)	0.80 ± 0.14	0.84 (0.74–0.89)	0.82 ± 0.09	0.91 (0.87–0.96)	0.91 ± 0.05
HNO_3/NO_y	16–37	0.03 (0.01–0.10)	0.05 ± 0.07	0.01 (0.00–0.02)	0.01 ± 0.02	< 0.01	< 0.01
PANs/NO_y	31	0.01 (0.00–0.03)	0.02 ± 0.04	no data		0.01 (0.00–0.02)	0.02 ± 0.01
NO_3^-/NO_y	30–31	0.01 (0.00–0.02)	0.01 ± 0.01	0.01 (0.00–0.04)	0.02 ± 0.02	0.03 (0.01–0.06)	0.03 ± 0.03
TN/NO_y	23–33	0.04 (0.01–0.12)	0.07 ± 0.07	0.02 (0.01–0.05)	0.03 ± 0.03	0.03 (0.01–0.06)	0.04 ± 0.03
ΔNO_y	102–273	2.1 (1.5–2.8)	2.4 ± 1.6	no data		1.6 (1.1–2.6)	2.8 ± 3.4
TN/NO_z	84–176	0.23 (0.16–0.30)	0.24 ± 0.16	no data		0.32 (0.23–0.42)	0.35 ± 0.18
PANs/NO_z	87–176	0.06 (0.03–0.09)	0.08 ± 0.07	no data		0.13 (0.09–0.18)	0.16 ± 0.12
$\Delta NO_y/NO_z$	132–323	0.69 (0.59–0.78)	0.67 ± 0.19	no data		0.50 (0.40–0.60)	0.49 ± 0.22
CO	5	260 (150–480)	300 ± 170	330 (230–490)	360 ± 160	480 (320–760)	560 ± 300
O_3	6–9	14 (2.8–39)	21 ± 22	17 (2.9–34)	20 ± 17	11 (1.7–27)	13 ± 11
Number of data (n)		4126		2056		2584	

[a]All the species concentrations units are in ppbv. The values in parentheses are 1σ values (central 67%).

soon after sunrise, reaching maximum values in the early afternoon, and decreased rapidly toward sunset. This diurnal pattern is similar to those for O_3 and $J(O^1D)$, suggesting that the concentrations of HNO_3 in urban air were mainly controlled by in situ photochemical production via reaction (R1) and removal-transport processes with similar time constants. The similarity of the production and accumulation between O_3 and HNO_3 was also shown in Figure 2. In winter, the

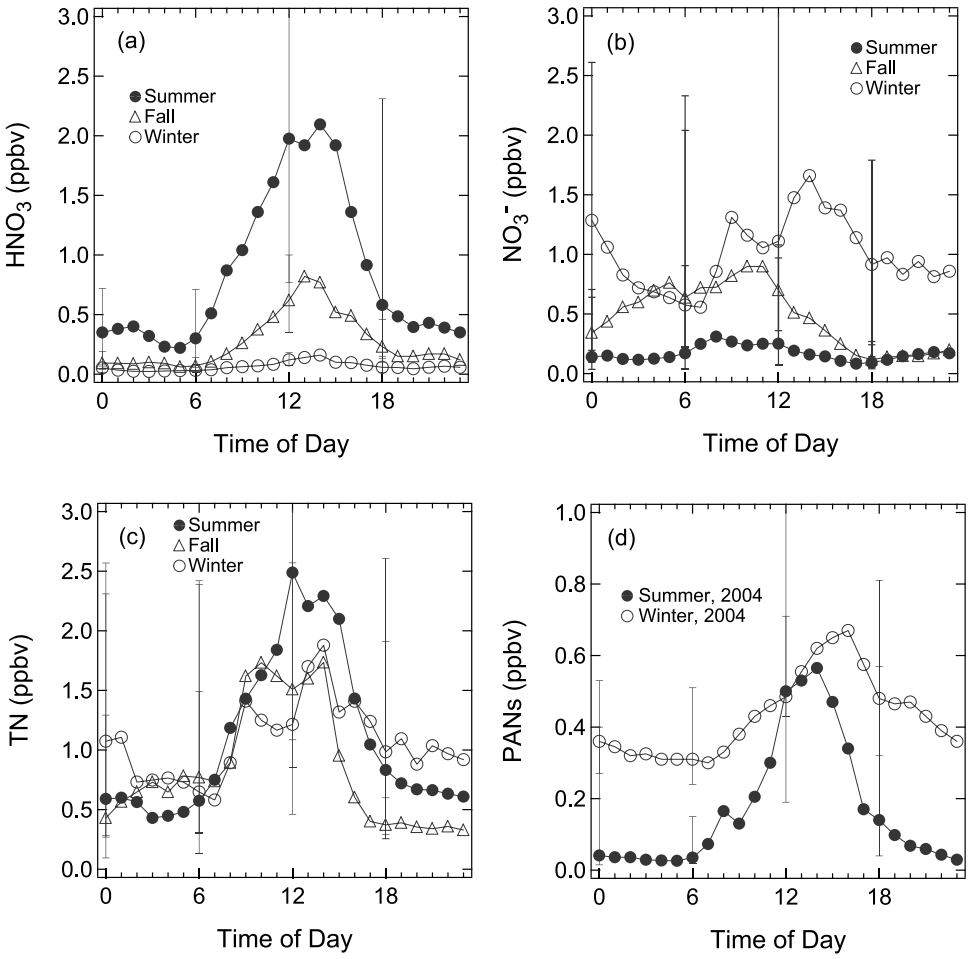

Figure 7. (a–d) Diurnal variations of the median values of the HNO_3, NO_3^-, TN = HNO_3 + NO_3^-, and PANs concentrations on HJ days in summer, fall, and winter. Bars represent 1σ values.

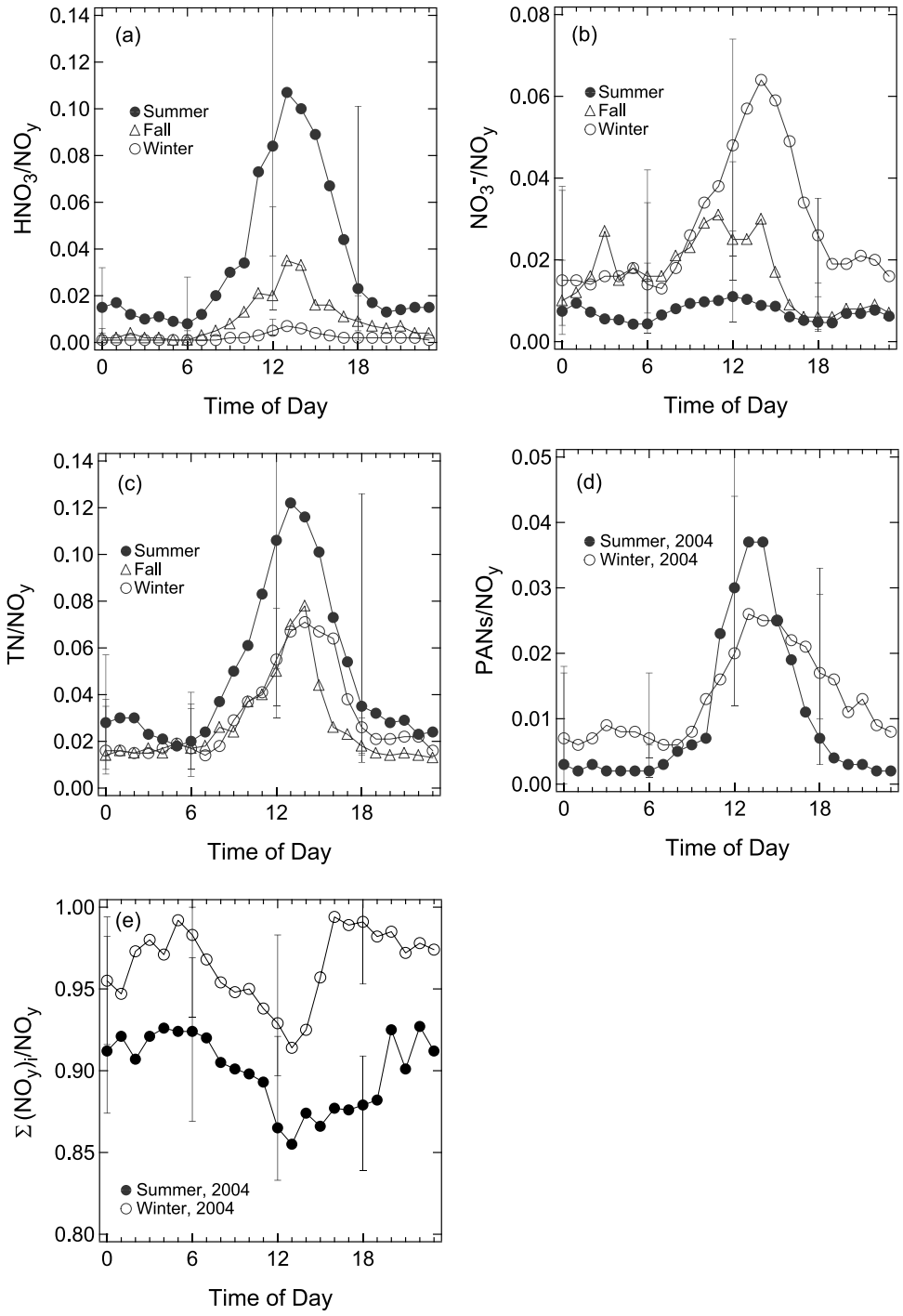

Figure 8. (a–e) Same as Figure 7 but for the HNO_3/NO_y, NO_3^-/NO_y, TN/NO_y, $PANs/NO_y$, and $\Sigma(NO_y)_i/NO_y$ ratios.

HNO_3 concentration showed little diurnal variation, with a median HNO_3 concentration of ~0.2 ppbv. It also showed little difference between HJ and LJ days (not shown).

[39] In contrast to the relatively regular diurnal variation of HNO_3, the NO_3^- concentrations showed rather irregular variations. In summer, NO_3^- peaked in the morning (0.3 ppbv), reached a minimum of < 0.1 ppbv in the late afternoon, and then increased again during the nighttime. The NO_3^- concentrations were much lower than those of HNO_3, especially during daytime. In fall, the diurnal patterns of HNO_3 and NO_3^- were similar to those in summer, although NO_3^- showed a broader peak (about 0.5–0.8 ppbv) from midnight to early afternoon. The HNO_3 concentration on LJ days (not shown) was lower than that on HJ days by a factor of 2, reflecting lower photochemical activity. In winter, the median NO_3^- concentrations (0.6–1.7 ppbv) were much higher than those of

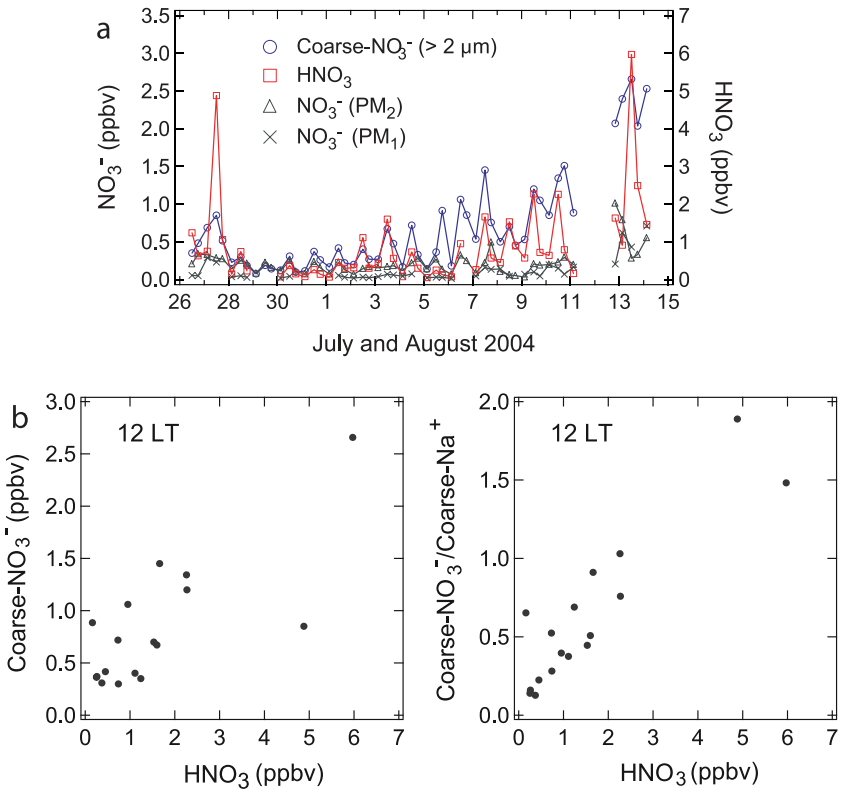

Figure 9. (a) Time series of the coarse- and PM_2-nitrate at TUMSAT and the PM_1-nitrate and HNO_3 at RCAST in the summer of 2004. (b) Correlation of the coarse-NO_3^- and coarse-NO_3^-/coarse-Na^+ ratio at TUMSAT with HNO_3 at RCAST in the summer of 2004.

HNO_3 (~0.2 ppbv). The NO_3^- concentrations on LJ days were comparable to or higher than that on HJ days.

[40] On HJ days, the HNO_3/NO_y and NO_3^-/NO_y ratios showed diurnal and seasonal variations similar to those for HNO_3, NO_3^-, and TN, as discussed above. Here we define $NO_z = NO_y - NO_x$ to represents the oxidized form of NO_x. As discussed in section 4.2, NO_x constituted a dominant fraction of NO_y. The uncertainty of NO_z is estimated to be as large as 82–174% owing to the subtraction of the two large terms. The median TN/NO_z ratios for summer and winter are shown in Table 5, together with their uncertainties. The median TN/NO_z ratios in winter were higher than those in summer. In summer $HNO_3 > NO_3^-$, and the median $HNO_3/NO_z \sim TN/NO_z = 0.23$. In winter, $NO_3^- \gg HNO_3$ and the median $NO_3^-/NO_z \sim TN/NO_z = 0.32$.

4.4. NO_3^- in Sea-Salt Particles

[41] Uptake of HNO_3 onto sea-salt particles (NaCl) has been suggested to be an important pathway of NO_y removal in marine and coastal areas [e.g., *Davies and Cox*, 1998; *Spokes et al.*, 2000]:

$$\text{(R7)} \quad HNO_3(g) + NaCl(s,\ aq) \rightarrow NaNO_3(s,\ aq) + HCl(g).$$

The uptake coefficient of HNO_3 onto sea-salt particles (dominated by NaCl) measured by laboratory experiments using an aerosol flow tube was 0.5 ± 0.2, which is much higher than that for mineral dust [*Guimbaud et al.*, 2002].

[42] Figure 9a shows variations of the concentrations of NO_3^- in the coarse mode (diameter larger than 2 μm), hereinafter denoted as coarse-NO_3^-, and NO_3^- (PM_2) measured at TUMSAT in summer 2004. The HNO_3 and NO_3^- (PM_1) concentrations measured at RCAST are also shown for comparison. The fine-mode NO_3^- (PM_1 and PM_2) was similar at these sites. It is likely that HNO_3 concentrations at TUMSAT were similar to those at RCAST considering that NO_3^- (PM_1) was nearly in equilibrium with HNO_3 at RCAST [*Morino et al.*, 2006]. PM_1-NO_3^- is nearly in equilibrium with HNO_3 and is a minor fraction of total nitrate during the daytime because of the high temperature.

[43] The coarse-NO_3^- concentrations showed distinct diurnal variations, with a peak in the early afternoon. They increased with the increase in HNO_3 and were much higher than PM_1-NO_3^- under high-HNO_3 conditions. This is seen more clearly by the correlation between coarse-NO_3^- and HNO_3 for 1200 LT, shown in the left plot of Figure 9b.

[44] The good correlation between HNO_3 and coarse-NO_3^- indicates that the flux of HNO_3 molecules onto sea-salt particles increased approximately in proportion to the HNO_3 concentrations, as predicted theoretically [*Seinfeld and Pandis*, 2006]. HNO_3 and coarse-NO_3^- will be correlated as long as the rate of HNO_3 deposition onto sea-salt particles does not far exceed the HNO_3 formation rate.

[45] The coarse-NO_3^-/HNO_3 ratios decreased under stagnant conditions in spite of the high HNO_3 concentrations. The right plot of Figure 9b shows the correlation between the HNO_3 concentration and the coarse-NO_3^-/coarse-Na^+ ratios. The good correlation even at the highest HNO_3 concentrations suggests that the concentration of sea-salt particles was also a limiting factor for the uptake of HNO_3

on sea-salt particles, especially at low-wind conditions. Except for these periods, the median coarse-NO_3^-/HNO_3 ratios were about 0.83 (1σ = 0.41–1.3), indicating significant removal of HNO_3 by uptake onto sea-salt particles. A large removal of HNO_3 by sea-salt particles was also suggested by a modeling study for Appledore Island, Maine, USA [*Fischer et al.*, 2006]. The uptake of HNO_3 onto sea-salt particles led to net NO_y removal, because coarse-NO_3^- was not included in NO_y, as discussed in section 2.2.

4.5. PANs

[46] The PANs concentrations and PANs/NO_y ratios underwent diurnal variations reaching maximum values in the afternoon on HJ days in summer and winter, as shown in Figures 7 and 8. The maximum median PANs/NO_y ratio was lower in winter (0.025) than in summer (0.04). The production rate of PANs is considered to have been higher in summer than in winter. However, the lifetime of PANs due to decomposition was shorter in summer (35 min) than in winter (14 h) for typical afternoon conditions. These compensating effects led to reduced seasonal variations of PANs. This point is discussed in more detail in section 5.

[47] The median PANs/NO_z ratios for summer and winter are shown in Table 5. The median PANs/NO_z ratios in winter (0.13) were higher than those in summer (0.06), opposite to the PANs/NO_y ratio.

4.6. $\Sigma(NO_y)_i$

[48] Here we compare the sum of the measured individual NO_y species ($(NO_y)_i$) with the directly measured total NO_y to understand pathways of NO_x oxidation in some more detail. The sum is defined as

$$\Sigma(NO_y)_i = NO_x + HNO_3 + NO_3^- + PANs, \quad (4)$$

and unmeasured NO_y (ΔNO_y) (or "missing NO_y") is defined as

$$\Delta NO_y = NO_y - \Sigma(NO_y)_i. \quad (5)$$

The uncertainties of $\Sigma(NO_y)_i$ and ΔNO_y in the three seasons were estimated to be about 13% and 103–273%, respectively, by combining possible errors of the individual measurements. The uncertainty of $\Sigma(NO_y)_i$ was derived as a root-sum-square of the uncertainty of each $(NO_y)_i$ species, weighted by its relative abundance. The much larger uncertainty of ΔNO_y is due to the subtraction of the two large terms in equation (5), similar to NO_z.

[49] $\Sigma(NO_y)_i$ was found to be highly correlated with NO_y, with linear regression slopes of 0.94 and 0.90 for the winter and summer periods, respectively. The average median $\Sigma(NO_y)_i/NO_y$ ratios were 0.89 ± 0.03 and 0.96 ± 0.02 (Figure 8). The $\Sigma(NO_y)_i/NO_y$ ratios showed a decrease during the daytime, and the minimum ratio was lower during summer than in winter. The seasonal variations of the median ΔNO_y and $\Delta NO_y/NO_z$ ratios are summarized in Table 5. The ratios of the sum of $RONO_2$ identified by gas chromatography ($\Sigma(RONO_2)_i$) to NO_y were less than 0.44%. The good correlation between ΔNO_y and NO_z (r^2 = 0.64) (not shown) suggests that ΔNO_y was produced photochemically. Both TN/NO_z and PANs/NO_z ratios were lower in summer than those in winters (Table 5), suggesting higher fraction of oxidized reactive nitrogen other than TN and PANs in summer. However, it should be stressed that the uncertainties of the $\Delta NO_y/NO_z$ ratios are very large (>100%), and quantitative discussion of ΔNO_y is not feasible.

[50] Total alkyl nitrates (ΣANs) have been measured using thermal dissociation followed by laser-induced fluorescence detection of NO_2 at rural and suburban sites in California and an urban site in Houston, Texas [*Day et al.*, 2002, 2003; *Rosen et al.*, 2004; *Cleary et al.*, 2005]. At the suburban and urban sites, the ΣANs/NO_y ratios were 0.1–0.25 in summer. The observed ΣANs were generally much higher than the sum of identified alkyl nitrates ($\Sigma(RONO_2)_i$) observed previously [e.g., *O'Brien et al.*, 1997] constituting a large fraction of the missing NO_y. Considering this, it is possible that ΣANs constituted a significant fraction of ΔNO_y also in the present observations.

[51] The oxidation of NO_x to ΣANs can significantly reduce NO_x lifetimes as compared with those estimated by considering only reaction (R1). In fact, lifetimes of NO_x in power plant and urban plumes were derived to be 2–5 h from the decay of NO_x in the plumes [*Ryerson et al.*, 1998, 2003; *Nunnermacker et al.*, 2000].

4.7. O_3 and $P(O_3)$

[52] According to the analysis by *Kanaya et al.* [2008], the predominant term in $F(O_3)$ is $k_{HO2+NO}[NO][HO_2]$ in general. The HO_2 concentration has been observed to be relatively stable at NO lower than 300 pptv decreasing with NO at higher NO as predicted for steady state conditions [*Kanaya et al.*, 2007] and predicted theoretically [*Seinfeld and Pandis*, 2006]. The observed dependence of HO_2 on NO also agreed with that predicted by the box model for the summer period. Because of this relationship, the dependence of $k_{HO2+NO}[NO][HO_2]$ on NO is much reduced with a broad maximum at NO mixing ratios of a few ppbv [*Kanaya et al.*, 2008]. However, for winter, the model underestimated the observed HO_2 at high NO. Therefore $P(O_3)$ estimated using the model-calculated HO_2 underestimated that derived using the observed HO_2, especially at NO mixing ratios larger than 10 ppbv. The $P(O_3)$ values shown in Figures 5 and 6 are those calculated using the observed HO_2.

[53] The O_3 concentrations showed maximum values in the early afternoon reaching close to zero just before sunrise in three seasons. However, the amplitudes of the diurnal variations of O_x were significantly smaller than that of O_3, because most of O_3 was converted to NO_2 during the nighttime, as seen from Figure 6. The importance of nighttime O_3 loss by NO_x titration in urban centers is well understood [e.g., *Sillman*, 1999]. It is likely that the seasonal variation of the regional background in O_3, which should be close to O_x, contributed to the seasonally different levels of the nighttime O_x. The surface O_3 at remote sites located at similar latitudes in Japan were reported to be about 40–50 ppbv in fall and winter and reach minimum values of about 25–35 ppbv [e.g., *Tanimoto et al.*, 2005; *Kondo et al.*, 2008]. In fall and winter, the background O_3 in the BL over Japan is strongly influenced by the Asian outflow and in summer it is influenced by inflow of cleaner maritime air. The daytime-nighttime difference in O_x is

Table 6. Background CO Concentrations[a]

	CO_{bkg} (ppbv)
Summer 2003	140
Fall 2003	106
Winter 2004	225
Summer 2004	98

[a]Lowest 1 Percentile.

largest in summer (about 30 ppbv) and smallest in winter (about 5 ppbv). Photochemical O_3 production during the daytime significantly contributed to the daytime increase in O_x, particularly in summer, as detailed below.

[54] The median of the daily peak $P(O_3)$ in winter was smaller than that in summer by only a factor 1.5 (about 12 ppbv h^{-1} versus 8 ppbv h^{-1}) despite the difference in HO_2 by about a factor of 6. This difference is due to the difference in NO by a factor of 3 around midday between winter and summer. The steady state $[NO]/[NO_y]$ ratio is expressed to a good approximation as

$$[NO]/[NO_y] = ([NO]/[NO_x])([NO_x]/[NO_y]) = (J(NO_2)/(J(NO_2) + k_{NO+O3}[O_3]))([NO_x]/[NO_y]). \quad (6)$$

In winter, NO_y and the NO_x/NO_y ratio were higher than in summer while O_3 was lower, leading to higher NO. It should be noted that if model-calculated HO_2 for winter is used, the compensating effect is much smaller and $P(O_3)$ has a more pronounced seasonal variation.

[55] In winter, the median $P(O_3)$ of about 5–6 ppbv h^{-1} at 0800–1300 LT is sufficient to cause the observed increase in O_x of about 5 ppbv over 0600–1300 LT on average. This does not exclude possible effects of dry deposition of O_3 during the daytime and transport in vertical and horizontal directions. In summer, the median $P(O_3)$ is also apparently sufficient to produce the median increase in O_x by about 30 ppbv from 0600 to 1200 LT. However, supply of larger O_x mixing ratios from above by convective mixing should also play a role, especially on stagnant conditions, as discussed in more detail in section 6.1.

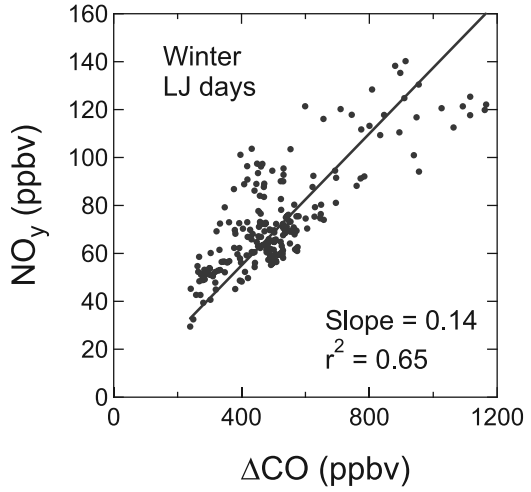

Figure 10. Correlation between NO_y and $\Delta CO = CO - CO_{bkg}$ (background CO) for LJ days in winter.

5. NO_x Oxidation and NO_y Removal

5.1. Estimate of NO_y Removal

[56] Here we estimate the remaining fractions of NO_y (R_{NOy}) in air masses sampled at RCAST, after transport from emission areas. For this purpose, CO was used as a tracer because CO is emitted simultaneously with NO_x and has a relatively long lifetime of 1–2 months. R_{NOy} is given as the ratio of the NO_y-CO correlation slope to the NO_x/CO emission ratio ($ER(NO_x/CO)$) [*Nunnermacker et al.*, 1998, 2000; *Koike et al.*, 2003; *Kondo et al.*, 2004]:

$$R_{NO_y} = (NO_y/\Delta CO)/ER(NO_x/CO). \quad (7)$$

[57] As discussed in section 2.1, NO_x is estimated to be emitted predominantly from motor vehicles, especially heavy-duty diesel vehicles in the TMA. $ER(NO_x/CO)$ was derived to be 0.24 for the TMA from the emission rates of NO_x and CO compiled by *Kannari et al.* [2004], although the uncertainties in the emission inventories were not estimated. Therefore, instead of using this ratio, $ER(NO_x/CO)$ was estimated using the observed NO_y and CO data. As a first step, we defined the background concentrations of CO (CO_{bkg}) as the values of the lowest 1 percentile for each season, as summarized in Table 6. ΔCO was then defined as $\Delta CO = CO - CO_{bkg}$. For estimating $ER(NO_x/CO)$, we used the NO_y and ΔCO data for LJ days in winter, when NO_x should be least oxidized. As discussed in section 3.1, the lifetime of NO_x on LJ days in winter was estimated to be about 7 days or longer. In fact, the median NO_x/NO_y ratios on LJ days in winter were as high as 0.89 even during the daytime. $ER(NO_x/CO)$ was estimated from (1) the median values of the $NO_y/\Delta CO$ ratios and (2) the slopes of the linear least squares regression of NO_y versus ΔCO. NO_y and ΔCO were highly correlated ($r^2 = 0.65$) with a slope of 0.14 ppbv/ppbv, as shown in Figure 10. $ER(NO_x/CO)$ for diesel vehicles has previously been reported to be much higher than that for gasoline vehicles [*Sawyer et al.*, 2000; *Marr et al.*, 2002] . The traffic density of diesel vehicles in the TMA generally reaches a maximum in the early morning [*Kondo et al.*, 2006]. Therefore, $ER(NO_x/CO)$ may undergo diurnal variations. Scatter in the slope of the NO_y-ΔCO correlation in Figure 10 includes this effect, and the 1 σ variability given in Table 5 gives the uncertainty in the derived $ER(NO_x/CO)$.

[58] In addition to the winter data, the median values of the $NO_y/\Delta CO$ ratios and the slopes were derived for the other seasons using the LJ data. The results are summarized in Table 7. There were no LJ days in the summer of 2004.

Table 7. Estimates of the NO_y/CO Emission Ratio

	Median $NO_y/\Delta CO$[a]	n	Slope of NO_y-ΔCO	r^2
Summer 2003	0.14 (0.12–0.23)	163	0.15	0.60
Fall 2003	0.14 (0.11–0.18)	106	0.13	0.82
Winter 2004	0.14 (0.12–0.18)	211	0.14	0.65

[a]The values in parentheses are 1σ values (central 67%) on $NO_y/\Delta CO$.

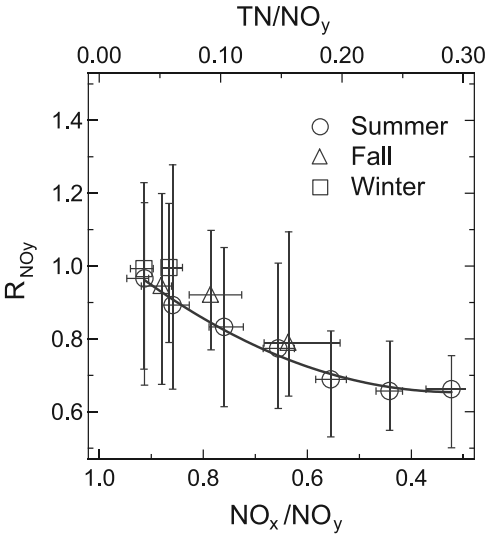

Figure 11. Correlation between the remaining fractions of NO_y (R_{NOy}) and the NO_x/NO_y (TN/NO_y) ratios for 0830–1730 LT on HJ days in summer (circles), fall (triangles), and winter (squares). The approximate TN/NO_y ratios, corresponding to the NO_x/NO_y ratios, are given for reference.

All the values are nearly identical irrespective of season, indicating that the value of 0.14 ppbv/ppbv is a valid estimate for $ER(NO_x/CO)$.

[59] It was found that $\Delta EC/\Delta CO$ ratios were lower by a factor 2 during the Bon holiday period of 12–14 August 2004, than those for the rest of the summer 2004 period. A likely explanation is that the ratio of diesel trucks to total vehicles in Tokyo was much lower during this period, when there was generally much less traffic. As stated above, emissions from diesel trucks are important sources of NO_y and EC in the TMA. A correction to $ER(NO_x/EC)$ was made using the change in the diesel trucks/total vehicles ratio estimated from the changes in the $\Delta EC/\Delta CO$ ratio, in a similar way to that described by *Kondo et al.* [2006]. The correction amounted to about 12%.

[60] The R_{NOy} estimated from equation (7) is plotted as a function of the NO_x/NO_y ratios for the daytime on HJ days in Figure 11. The data were binned according to the NO_x/NO_y ratio and the median R_{NOy} for each bin was derived from the NO_y-CO correlation. The approximate TN/NO_y ratios are also shown for reference. The median values of R_{NOy} for each season are summarized in Table 8. The slope of the R_{NOy}-NO_x/NO_y correlation depends strongly on the relative rate of the depositional removal of HNO_3 to the NO_x oxidation rate. Generally, faster HNO_3 removal leads to a steeper slope, which therefore can be sensitive to dry deposition rates of HNO_3.

[61] R_{NOy} decreased with the decrease in the NO_x/NO_y ratio in summer and fall. Because the NO_x/NO_y ratio decreased from early morning to the early afternoon, the change in R_{NOy} in Figure 11 also represents the diurnal variation of R_{NOy} in each season. On average between 0830 and 1730 LT, the R_{NOy} values were estimated to be 0.78, 0.90, and 1.0 for the summer, fall, and winter periods, respectively.

[62] The systematic decrease in R_{NOy} with the decrease (increase) in the NO_x/NO_y (TN/NO_y) ratios in summer is likely due to the removal of NO_y through production of HNO_3 and its subsequent removal (high HNO_3/TN ratios). The removal of HNO_3 can occur by dry deposition and uptake on sea-salt particles. Precipitation occurred only on one day both in summer and winter. The coarse-NO_3^-/NO_y ratio was about 7% under weak wind conditions in summer, suggesting that the uptake of HNO_3 on sea-salt particles contributed to the removal of NO_y by a similar degree. In fall, a similar trend was seen, although the range of the TN/NO_y ratios was narrower. In winter, NO_x/NO_y ratios were about 0.9 and the R_{NOy} was close to 1. The uncertainties in R_{NOy} were largely due to the diurnal variation of $ER(NO_x/CO)$, which reached maximum and minimum values in the early morning and afternoon, respectively (not shown).

5.2. Estimate of NO_x Oxidation

[63] Here we derive the NO_x oxidation, formation of NO_z, and removal of NO_y for summertime conditions, relative to the NO_x emitted. For this purpose, we first estimate NO_y mixing ratios uninfluenced by irreversible removal (NO_y^*) as a function of the observed CO (or ΔCO) using ER (NO_x/CO). NO_y^* is given as

$$NO_y^* = \Delta CO \times ER(NO_x/CO). \quad (8)$$

The ratio of removed NO_y (δNO_y) to NO_y^* is given as

$$\delta NO_y/NO_y^* = 1 - R_{NOy}. \quad (9)$$

[64] Figure 12 shows the median NO_x/NO_y^*, NO_z/NO_y^*, and $\delta NO_y/NO_y^*$ ratios as functions of the NO_x/NO_y ratio. The approximate residence time (*RT*), as derived in Appendix A is also shown as a reference. On LJ days in summer, the NO_x/NO_y ratios were about 0.89, as discussed in section 3 (Figure 6). In these air masses, about 89% (100%) of the emitted NO_x (NO_y) remained. These data represent less-processed air.

[65] On HJ days, the median NO_x/NO_y ratios were about 0.89 in the morning and late afternoon (around 1000 and 1700 LT), representing moderately processed air. During daytime (1000–1700 LT), the ratios decreased to about 0.78, representing highly processed air. The remaining portions of NO_x (NO_y) were about 76% (86%) and 66% (84%) for moderately and highly processed air, respectively. In highly processed air, 18% of the emitted NO_x remained as NO_z and 16% of NO_y was removed.

[66] During the stagnant conditions of 12–14 August, with an *RT* of 8–10 h (Appendix A), the NO_x/NO_y ratios decreased to as low as 0.44. Substantial oxidation of NO_x (69%) and removal of NO_y (30%) occurred in this extremely processed air. These results indicate that most of the

Table 8. Remaining Fractions of NO_y (R_{NOy}) During the Daytime and the Nighttime on HJ Days

	0830–1730 LT	1730–0830 LT
Summer	0.78 (0.62–0.94)	0.86 (0.67–1.02)
Fall	0.90 (0.70–1.06)	0.96 (0.75–1.12)
Winter	1.00 (0.84–1.26)	0.93 (0.77–1.16)

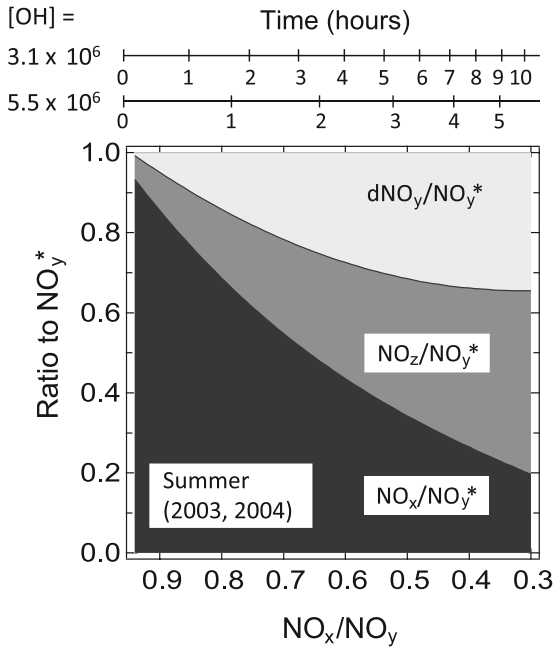

Figure 12. Ratios of δNO_y (NO_y removed), $NO_z = NO_y - NO_x$, and NO_x to NO_y^* (estimated NO_y uninfluenced by removal) versus the NO_x/NO_y ratio on HJ days in summer. Approximate residence times assuming average OH concentrations of 5.5×10^6 and 3.1×10^6 cm^{-3} are also shown for reference.

emitted NO_x was lost within 10 h even in urban areas in summer.

[67] By contrast, in winter little NO_y was removed during any conditions within the error of the estimate (Figure 12), although about 15% of the emitted NO_x was converted to NO_z during the daytime of HJ days. The majority of the TN was in the form of NO_3^- owing to the low temperature, leading to significantly reduced NO_y removal.

6. Formation of O_3, PAN, TN, and SOA in Summer

6.1. High O_3, PANs, and SOA During Phase 2

[68] Here we investigate key processes that caused enhanced O_x and PANs on 12–14 August, when a stagnant sea-land circulation developed. Both PANs and O_x mixing ratios were much higher than those during the preceding period, as discussed in section 3.2. HO_2 also showed a large increase during the daytime as predicted by the increase in O_3. $P(O_3)$ reached maximum values of about 10–15 ppbv h^{-1} around midday on these days. However, $P(O_3)$ did not show significant variability throughout phases 1 and 2 because NO was low in the early afternoon when HO_2 reached maximum (Figure 2b). As a result, the $P(O_3)$ values on the high-O_x days are close to the median value for the summertime. The low NO in the early afternoon was mainly due to the reduced NO/NO_x and NO_x/NO_y ratios (Figure 2b). The high O_3 mainly lowered the NO/NO_x ratios. The low NO_x/NO_y ratios (as low as 0.3) could have been due to oxidation of NO_x in stagnant air near the surface and partly due to downward transport of aged air by vertical mixing, and the reduced NO_x emissions due to the Bon holidays (section 5.1). The NO levels on these days were significantly lower than those on the other days for comparable levels of VOCs [*Kanaya et al.*, 2008, Figure 7] and $P(O_3)$ was NO_x-limited in these cases.

[69] As anticipated from the trajectories shown in Figure 3, the air mass sampled in the early afternoon accumulated primary pollutants from the previous night. In fact peaks in NO_y (Figure 2a) and VOCs (C_2H_4 and C_2H_6) [*Shirai et al.*, 2007] were seen during the peak in O_3. However, it is very unlikely that the enhanced levels of these species led to significant increases in $P(O_3)$, as discussed above. Considering that air masses stayed at locations close to RCAST, the diurnal variation of $P(O_3)$ shown in Figure 2b should be close to that for air masses sampled in the early afternoon. Accumulation of O_3 produced after sunrise is insufficient to explain the observed O_x increase by up to 104–116 ppbv from 0500 to 1300 LT [*Kanaya et al.*, 2008]. Instead, it is likely the high O_x was due to the accumulation of O_x from previous days at higher altitudes in the BL and to transport down to near the surface by mixing. The very low NO_x/NO_y ratios could have been due, at least partly, to downward transport of aged air by vertical mixing, although its relative importance is not quantified.

[70] The enhancement of O_3 occurred not only at RCAST but also over a wide region of the TMA on 12–14 August. In Kisai and the northern part of the TMA, midday O_3 exceeded 80 ppbv after 9 August [*Miyakawa et al.*, 2008], two days earlier than at RCAST. Considering that $P(O_3)$ was rather insensitive to the NO_x level and following the same reasoning discussed above, the observed high O_3 (>80 ppbv) in Kisai also cannot be explained solely by in situ O_3 formation. The wind fields shown by *Shirai et al.* [2007] suggest that the air over the entire TMA was under the influence of sea-land breeze circulation. *Wakamatsu et al.* [1983, 1996, 1999] have shown the effect of accumulation of O_3 in elevating its concentrations over the TMA under sea-land breeze circulation conditions using field observations and modeling studies. In particular, they observed O_3 mixing ratios exceeding 80 ppbv above the surface (0.2–1.2 km) over a wide region of TMA under the stagnant conditions in summer of 1978.

[71] In Figure 13, the observed concentration of saturated PANs (PAN + PPN + PiBN + PnBN) is compared with model simulations. The model predicted the observed PANs quite well during phase 1. However, the model underestimated enhanced PANs concentrations observed during phase 2, especially on 12–14 August. Model calculations were also made by varying the ALD (acetaldehyde and higher aldehydes in RACM) concentrations to estimate the sensitivity of the calculated PANs to ALD, because the ALD concentrations can be highly uncertain. The calculated PANs with the ALD tripled still cannot explain the observations. The ALD concentrations calculated without the ALD constraint was about 70% of the ALD concentrations used for the standard model run, suggesting that the uncertainty in ALD concentrations is smaller than a factor of 3. In the model, ACO3 (acetyl peroxy and higher saturated acyl peroxy radicals in RACM) is the precursor of PAN. It is mainly produced by the ALD-OH reaction and photolysis of MGLY (methylglyoxal and other α-carbonyl aldehydes). In turn, ALD was mainly produced from

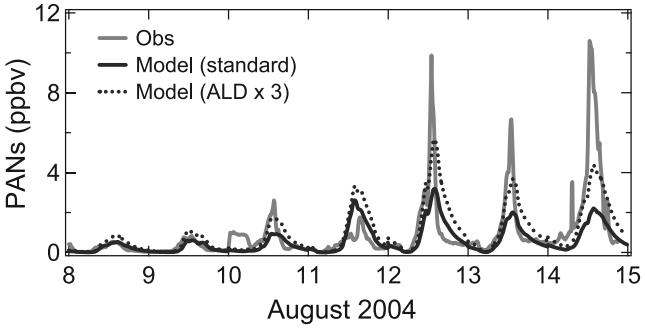

Figure 13. Temporal variations of observed (black line) and simulated (gray line) PANs concentrations in the summer of 2004. The results from two model runs are included: one with the acetaldehyde and higher aldehydes (ALD) concentrations constrained at standard levels (solid line) and the other with those tripled (dotted line). See text for more details.

oxidation of olefins and alkanes (including alcohols) and MGLY originating from oxidation of aromatics.

[72] The daytime maximum concentrations on the highest PANs days were reproduced by the model by employing temperatures 9°C lower than at ground level (corresponding to 0.9 km), increasing ALD concentrations by a factor of 3, and increasing time constant for dilution (48 h) simultaneously. The longer time constant may represent the stagnant conditions (increased horizontal homogeneity in the BL). Considering these comparisons, it may be possible that the high PANs concentrations observed at the surface were due to downward transport of the upper BL with lower temperatures and augmented aldehyde concentrations due to stagnation.

6.2. O_3-PANs-TN-SOA Correlations

[73] Correlations between the species photochemically produced are shown in Figure 14. The correlations were tighter for O_x than O_3 (not shown). The slope of the PANs-O_x correlation for O_x lower than 60 ppbv, mainly during phase 1, was lower than that for O_x higher than 80 ppbv. A similar feature was observed for TN. At lower O_x (higher wind speed), the local productions and loss should control the PANs and TN concentrations. At higher O_x (lower wind speed), accumulated aldehydes (section 6.1) and TN in the entire BL may have caused steeper slopes of the PANs-O_x and TN-O_x correlations.

[74] Both oxygenated organic aerosol (OOA) and OA correlated well with O_x (r^2 = 0.74 and 0.79, respectively). OOA and hydrocarbon-like organic aerosol (HOA) were quantified from AMS mass spectral time series using an algorithm based on a custom principal component analysis

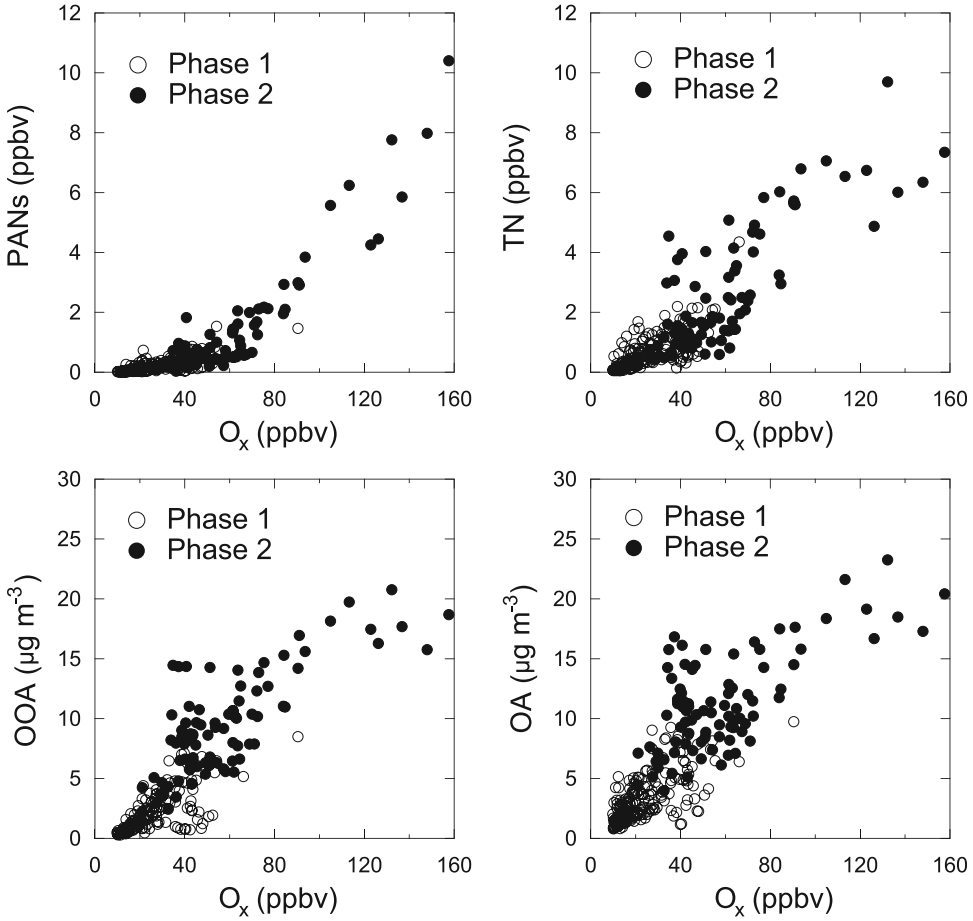

Figure 14. Correlations of PAN, total nitrate (TN), oxygenated organic aerosol (OOA), and organic aerosol (OA) with $O_x = O_3 + NO_2$ in summer 2004.

[*Kondo et al.*, 2007]. About 90% of OOA was estimated to be water soluble for summer and winter, indicating that OOA represents SOA. In summer, OA and OOA were tightly correlated ($r^2 = 0.95$), and the OOA/OA ratio was about 0.8 owing to high levels of photochemical activity, which led to active formation of SOA. Correlation of OA with O_3 at RCAST in summer has been reported by *Takegawa et al.* [2006a]. Figure 14 demonstrates tighter correlations of OA and OOA with O_x than with O_3. More importantly, the OA-O_x correlation was linear throughout the whole O_x range. This is because OA is more highly conserved than PANs and TN owing to its much slower dry deposition velocity. The tight OA-O_x correlation indicates that the accumulation and mixing processes led to simultaneous increases in O_3 (>about 80 ppbv) and SOA (>15 μg m^{-3}).

7. Summary and Conclusions

[75] Simultaneous measurements of major components of reactive nitrogen (NO_x, PANs, HNO_3, and NO_3^- (PM_1)), total reactive nitrogen (NO_y), VOCs, and HO_x were made at RCAST, located near the urban center of Tokyo in summer, fall, and winter 2003–2004 to study the processes involving oxidized forms of reactive nitrogen and O_3. The median NO_y concentrations were about 20–42 ppbv during these periods. On average, the $\Sigma(NO_y)_i/NO_y$ ratios were 0.96 ± 0.02 and 0.89 ± 0.03 in winter and summer, respectively, confirming the overall validity of the measurements of the NO_y species.

[76] The median NO_x/NO_y ratios underwent distinct diurnal variations in each season reaching minimum values in the early afternoon on HJ days, owing to the oxidation of NO_x by OH (reaction (R1)). The daily minimum NO_x/NO_y ratios were lower in summer (about 0.7) than those in winter (about 0.85), reflecting faster oxidation of NO_x due to the higher OH concentrations. On LJ days, the median NO_x/NO_y ratios showed little diurnal variation and remained high (mostly above 0.8), irrespective of season, consistent with the longer lifetime of NO_x.

[77] In summer, the dominant form of TN was HNO_3, with a maximum at 1400 LT. The coarse-NO_3^- concentrations, which were not included in NO_y, increased nearly in proportion to the HNO_3 concentrations. This implies that a significant fraction of HNO_3 was taken up by sea-salt particles. In winter, NO_3^- was the dominant form of TN. The lower HNO_3 and higher NO_3^- in winter were due to the shift of the HNO_3-NO_3^- partitioning to NO_3^- at low temperatures.

[78] The nighttime levels of O_x were much higher in fall and winter than those in summer reflecting the seasonal variation of the background O_3. The daytime-nighttime difference in O_x was largest in summer (about 30 ppbv) and smallest in winter (about 5 ppbv) in winter. Photochemical O_3 production during the daytime partly contributed to the daytime increase in O_x, consistent with the estimated $P(O_3)$. In addition to the O_3 formation, dry deposition of O_3 during the daytime and transport in vertical and horizontal directions should have played some roles in controlling the seasonal-diurnal variation of O_x.

[79] The remaining fraction of NO_y (R_{NOy}) was estimated from the decrease in the slope of the observed NO_y-CO correlation from the estimated NO_x/CO emission ratios. R_{NOy} decreased with the decrease in the NO_x/NO_y ratio in summer and fall. The systematic decrease in R_{NOy} with the decrease in the NO_x/NO_y ratios was likely due to the removal of NO_y through production of HNO_3 and its subsequent removal. The removal of HNO_3 could have occurred by dry deposition and uptake on sea-salt particles. On average during 0830–1730 LT, the R_{NOy} values were 0.78 and 0.90 for summer and fall, respectively. Little NO_y was removed in winter owing to the suppressed HNO_3 production.

[80] The median NO_x/NO_y ratios of 0.89 (LJ days), 0.89 (morning and late afternoon-nighttime on HJ days), 0.78 (daytime on HJ days), and 0.44 (daytime under stagnant conditions in summer) represent air masses with different degrees of photochemical processing. The remaining fractions of NO_x (NO_y) in these air masses were estimated to be about 89 (100), 76 (86), 66 (84), and 31 (70) %, respectively. These remaining NO_x amounts give initial conditions that control the transport of NO_x from the urban center of the TMA to its surrounding regions.

[81] Under stagnant conditions on 12–14 August in 2004, O_x increased up to 150–170 ppbv by early afternoon. Accumulation of O_3 produced after sunrise is insufficient to explain the observed O_x increase. It is likely that the high O_x was due to the accumulation of O_x from previous days at higher altitudes in the BL followed by transport down to near the surface by mixing. Vertical mixing could have also contributed to the large increase in PANs during midday on these days.

[82] SOA was highly correlated with O_x. It is likely that O_x and SOA accumulated during the course of sea-land breeze circulation above the surface in the BL and were transported to the surface together with O_x. The identification of the importance of vertical transport for high O_x (>80 ppbv) and other oxidants is important in predicting secondary oxidants in the TMA and their future reductions.

Appendix A: Oxidation of NO_x

[83] We have shown in section 4 that reaction (R1) and oxidation to PAN were the major pathways of the oxidation of NO_x during the daytime. In this section, we interpret the decrease in NO_x observed in summer more quantitatively by taking into account the oxidation process during transport that occurred prior to sampling air masses at RCAST. Changes in NO_x concentrations due to reaction (R1) are expressed as

$$\begin{aligned} d[NO_x]/dt &= -k_{OH+NO2}[OH][NO_2] \\ &= -k_{OH+NO2}[OH][NO_x]([NO_2]/[NO_x]). \end{aligned} \quad (A1)$$

Here we neglect the effect of PAN formation for simplicity and discuss this point in the interpretation of the results. The NO_x concentrations at time t ($NO_x(t)$) after NO_x emissions beginning at $t = 0$ can be expressed by

$$NO_x(t)/NO_x(0) = \exp\left(-\int k_{OH+NO2}[OH]([NO_2]/[NO_x])dt\right). \quad (A2)$$

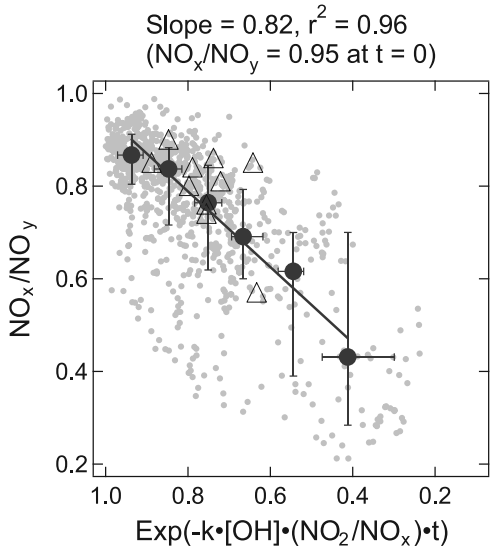

Figure A1. Correlation of the NO_x/NO_y ratio with the fraction of remaining NO_x estimated as $\exp(-k_1[OH]([NO_2]/[NO_x])t)$ on HJ days in summer. The slope and r^2 for the correlation for the binned $\exp(-k_1[OH]([NO_2]/[NO_x])t)$ values are 0.82 and 0.96, respectively. The slope and r^2 using all the data points are 0.69 and 0.48, respectively. The data points, for which photochemical ages were obtained, are depicted as triangles.

If average OH concentrations and $[NO_2]/[NO_x]$ ratios are used for simplicity, equation (A2) is reduced to

$$NO_x(t)/NO_x(0) = \exp(-k_{OH+NO2}[OH]([NO_2]/[NO_x])t). \quad (A3)$$

[84] For the present calculations, the reaction time t was given as the residence time (*RT*) of the sampled air mass in the high-NO_x emission areas. Spatial variability of the NO_x emission rates in the in high-emission areas is relatively small and is not a large source of uncertainty. However, considering that NO_x was injected into the sampled air masses continuously during their transport, the *RT*s derived in this way may be overestimates.

[85] Figure 3 shows typical backward trajectories of air masses arriving at RCAST during summer, overlaid with the emission rates of NO_x. The backward trajectories were calculated using the wind data obtained at RCAST, because the winds in summer were generally southerly during the daytime owing to the sea breeze in the high-NO_x area. The high-emission areas in the study region are marked in red. Spatial inhomogeneity of wind fields within the high-NO_x areas introduced some errors in the trajectory calculations. The wind speeds measured by Japan Meteorological Agency at Yokohama (30 km south of RCAST) and Nerima (10 km north of RCAST) were stronger and weaker by factors 2.2 and 0.65, respectively than those at RCAST on these days on average. The wind directions at Yokohama and Nerima were to within ±28° of those at RCAST. However, it is very difficult to estimate errors in *RT* by this inhomogeneity, because of the complexity of a wind system of this scale.

[86] The backward trajectory for 2 August is typical for the observational period from 1–9 August 2004. Air masses arriving at RCAST remained in the high-emission areas for a few hours. On the other hand, the backward trajectory for 13 August is typical for 10–14 August. The air masses stagnated owing to the development of the sea-land breeze circulation, and the air masses sampled at RCAST remained in the emission areas for about 10 h. The *RT* values estimated for the summer period typically range over 1.5–6.0 h.

[87] The photochemical ages (*PA*) of air masses can be estimated using the ratio of alkyl nitrates to their parent hydrocarbons [*Bertman et al.*, 1995]. For the present analysis, the ratio of 2-pentyl nitrate (2-$PeONO_2$) to *n*-pentane (*n*-C_5H_{12}) was chosen [*Simpson et al.*, 2003; *Takegawa et al.*, 2006b]. The 2-$PeONO_2$/*n*-C_5H_{12} ratio and *PA* (or t) are related as

$$\frac{[2\text{-}PeONO_2]}{[n\text{-}C_5H_{12}]} = \frac{\beta k_A}{(k_B - k_A)}\left(1 - e^{(k_A - k_B)t}\right), \quad (A4)$$

where β is the fractional yield, and k_A and k_B are the pseudo-first-order rate coefficients for the formation and destruction of 2-$PeONO_2$, respectively. Values of these parameters for typical midlatitude surface conditions during spring were given by *Simpson et al.* [2003]. The coefficient k_B is a function of [OH]. We assumed average values of [OH] = 5.5×10^6 cm^{-3} (1000–1500 LT) and 3.1×10^6 cm^{-3} (0500–1900 LT), which gave *RT*/*PA* ratios of 1.6 ± 0.80 and 1.2 ± 0.6, respectively, with r^2 = 0.31 for the *RT*-*PA* correlation. The results showing *RT*/*PA* ratios larger than 1 are consistent with the possible overestimation of *RT*, although other factors, including effects of vertical mixing, also introduce additional uncertainties. These results suggest *RT* can be used as a qualitative measure of air mass age. The uncertainties discussed above will be greatly reduced if the plumes are well defined, as has been done for aircraft studies of plumes from power plants [e.g., *Nunnermacker et al.*, 1998, 2000; *Neuman et al.*, 2002, 2004].

[88] Using the *RT*, we investigate the validity of equation (A3). If NO_y is conserved, $NO_x(0) = NO_y$. Figure A1 shows the relationships between the observed NO_x/NO_y ratios with the $\exp(-k_1[OH]([NO_2]/[NO_x])t)$ value calculated for the average [OH] = 5.5×10^6 cm^{-3} (1000–1500 LT). The data points for which the *PA* values were obtained are depicted as triangles. The median NO_x/NO_y ratios for each bin are correlated well with $\exp(-k_1[OH]([NO_2]/[NO_x])RT)$ (r^2 = 0.96) with a slope of 0.82. The scatter of the correlation can arise partly from the uncertainties in the estimate of *RT*, as discussed above.

[89] Some fractions of NO_y were found to have been removed during transport, as discussed in section 6.1. A NO_y value that was corrected for this removal, denoted NO_y^*, was also used for $NO_x(0)$ for comparison. Using the NO_y^* values did not significantly alter the correlation (r^2 = 0.91) and slope (=0.85). The correction by NO_y^* becomes important for the lowest NO_x/NO_y ratios. Because the fraction of these data is small, the NO_y^* correction is not important in this case. It should be noted that NO_x lost to PANs is not considered in equation (1). The time constant of PAN formation is different from HNO_3 formation, although reactions of OH with VOCs are involved in PANs formation. In addition, formation of alkyl nitrate is also an important pathway for NO_x oxidation [e.g., *Day et al.*,

2003], as discussed in section 4.6. Therefore, the term $\exp(-k_{OH+NO2}[OH]([NO_2]/[NO_x])t)$ should be considered to represent a qualitative measure of chemical aging of NO_x, rather than a quantitative measure of NO_x oxidation. In practice, the reasonably good correlation of this term with the NO_x/NO_y ratios and the slope of 0.82 suggests that the NO_x/NO_y ratios approximately represent air mass ages due to oxidation along trajectories.

[90] **Acknowledgments.** This work was supported by the Ministry of Education, Culture, Sports, Science, and Technology (MEXT), the global environment research fund of the Japanese Ministry of the Environment (B-083), and the Japanese Science and Technology Agency (J. S. T.). We thank I. J. Simpson for providing critical comments on this paper. We also thank Y. Komazaki for assistance in the field experiments.

References

Bertman, S. B., J. M. Roberts, D. D. Parrish, M. P. Buhr, P. D. Goldan, W. C. Kuster, and F. C. Fehsenfeld (1995), Evolution of alkyl nitrates with air mass age, *J. Geophys. Res.*, *100*, 22,805–22,813.

Blake, N. J., D. R. Blake, A. L. Swanson, E. Atlas, F. Flocke, and F. S. Rowland (2003a), Latitudinal, vertical, and seasonal variations of C_1–C_4 alkyl nitrates in the troposphere over the Pacific Ocean during PEM-Tropics A and B: Oceanic and continental sources, *J. Geophys. Res.*, *108*(D2), 8242, doi:10.1029/2001JD001444.

Blake, N. J., D. R. Blake, B. C. Sive, A. S. Katzenstein, S. Meinardi, O. W. Wingenter, E. L. Atlas, F. Flocke, B. A. Ridley, and F. S. Rowland (2003b), The seasonal evolution of NMHCs and light alkyl nitrates at middle to high northern latitudes during TOPSE, *J. Geophys. Res.*, *108*(D4), 8359, doi:10.1029/2001JD001467.

Cleary, P. A., J. G. Murphy, P. J. Wooldridge, D. A. Day, D. B. Millet, M. McKay, A. H. Goldstein, and R. C. Cohen (2005), Observations of total alkyl nitrates within the Sacramento urban plume, *Atmos. Chem. Phys. Disc.*, *5*, 4801–4843.

Davies, J. A., and R. A. Cox (1998), Kinetics of the heterogeneous reaction of HNO_3 with NaCl: Effect of water vapor, *J. Phys. Chem. A*, *102*, 7631–7642, doi:10.1021/jp982134t.

Day, D. A., P. J. Wooldridge, M. B. Dillon, J. A. Thornton, and R. C. Cohen (2002), A thermal dissociation laser-induced fluorescence instrument for in situ detection of NO_2, peroxy nitrates, alkyl nitrates, and HNO_3, *J. Geophys. Res.*, *107*(D6), 4046, doi:10.1029/2001JD000779.

Day, D. A., M. B. Dillon, P. J. Wooldridge, J. A. Thornton, R. S. Rosen, E. C. Wood, and R. C. Cohen (2003), On alkyl nitrates, O_3, and the "missing NO_y", *J. Geophys. Res.*, *108*(D16), 4501, doi:10.1029/2003JD003685.

de Gouw, J. A., et al. (2005), Budget of organic carbon in a polluted atmosphere: Results from the New England Air Quality Study in 2002, *J. Geophys. Res.*, *110*, D16305, doi:10.1029/2004JD005623.

DeMore, W. B., S. P. Sander, C. J. Howard, A. R. Ravishankara, D. M. Golden, C. E. Kolb, R. F. Hampson, M. J. Kurylo, and M. J. Molina (1997), Chemical kinetics and photochemical data for use in stratospheric modeling, *Eval. 12*, Jet Propul. Lab., Calif. Inst. of Technol., Pasadena.

Ehhalt, D. H., and F. Rohrer (2000), Dependence of the OH concentration on solar UV, *J. Geophys. Res.*, *105*, 3565–3571.

Fahey, D. W., G. Hübler, D. D. Parrish, E. J. Williams, R. B. Norton, B. A. Ridley, H. B. Singh, S. C. Liu, and F. C. Fehsenfeld (1986), Reactive nitrogen species in the troposphere: Measurements of NO, NO_2, HNO_3, particulate nitrate, peroxyacetyl nitrate (PAN), O_3, and total reactive odd nitrogen (NO_y) at Niwot Ridge, *J. Geophys. Res.*, *91*, 9781–9793.

Fehsenfeld, F. C., et al. (1987), A ground-based intercomparison of NO, NO_x, and NO_y measurement techniques, *J. Geophys. Res.*, *92*, 14,710–14,722.

Fischer, E., A. Pszenny, W. Keene, J. Maben, A. Smith, A. Stohl, and R. Talbot (2006), Nitric acid phase partitioning and cycling in the New England coastal atmosphere, *J. Geophys. Res.*, *111*, D23S09, doi:10.1029/2006JD007328.

Griffin, R. J., D. R. Cocker III, R. C. Flagan, and J. H. Seinfeld (1999), Organic aerosol formation from the oxidation of biogenic hydrocarbons, *J. Geophys. Res.*, *104*, 3555–3567.

Guimbaud, C., F. Arens, L. Gutzwiller, H. W. Gäggeler, and M. Ammann (2002), Uptake of HNO_3 to deliquescent sea-salt particles, *Atmos. Chem. Phys. Disc.*, *2*, 739–763.

Guttikunda, S. K., Y. Tang, G. R. Carmichael, G. Kurata, L. Pan, D. G. Streets, J. H. Woo, N. Thongboonchoo, and A. Fried (2005), Impacts of Asian megacity emissions on regional air quality during spring 2001, *J. Geophys. Res.*, *110*, D20301, doi:10.1029/2004JD004921.

Harder, J. W., J. W. Brault, P. V. Johnston, and G. H. Mount (1997), Temperature dependent NO_2 cross sections at high spectral resolution, *J. Geophys. Res.*, *102*(D3), 3861–3879.

Hoffmann, T., J. R. Odum, F. Bowman, D. Collins, D. Klockow, R. C. Flagan, and J. H. Seinfeld (1997), Formation of organic aerosols from the oxidation of biogenic hydrocarbons, *J. Atmos. Chem.*, *26*, 189–222, doi:10.1023/A:1005734301837.

Kalberer, M., J. Yu, D. R. Cocker, R. C. Flagan, and J. H. Seinfeld (2000), Aerosol formation in the cyclohexene-ozone system, *Environ. Sci. Technol.*, *34*, 4894–4901, doi:10.1021/es001180f.

Kanaya, Y., Y. Sadanaga, J. Hirokawa, Y. Kajii, and H. Akimoto (2001a), Development of a ground-based LIF instrument for measuring HO_x radicals: Instrumentation and calibrations, *J. Atmos. Chem.*, *38*, 73–110, doi:10.1023/A:1026559321911.

Kanaya, Y., Y. Sadanaga, K. Nakamura, and H. Akimoto (2001b), Behavior of OH and HO_2 radicals during the observations at a Remote Island of Okinawa (ORION99) field campaign: 1. Observation using a laser-induced fluorescence instrument, *J. Geophys. Res.*, *106*, 24,197–24,208.

Kanaya, Y., R. Cao, H. Akimoto, M. Fukuda, Y. Komazaki, Y. Yokouchi, M. Koike, H. Tanimoto, N. Takegawa, and Y. Kondo (2007), Urban photochemistry in central Tokyo: 1. Observed and modeled OH and HO_2 radical concentrations during the winter and summer of 2004, *J. Geophys. Res.*, *112*, D21312, doi:10.1029/2007JD008670.

Kanaya, Y., M. Fukuda, H. Akimoto, N. Takegawa, Y. Komazaki, Y. Yokouchi, M. Koike, and Y. Kondo (2008), Urban photochemistry in central Tokyo: 2. Rate and regimes of oxidant (O_3 + NO_2) production, *J. Geophys. Res.*, *113*, D06301, doi:10.1029/2007JD008671.

Kannari, A., T. Baba, H. Ueda, Y. Tonooka, and K. Matsuda (2004), Development of a grid database on atmospheric pollutants emissions in Japan (in Japanese), *J. Jpn. Soc. Atmos. Environ.*, *39*(6), 257–271.

Kita, K., et al. (2006), A chemical ionization mass spectrometer for ground-based measurement of nitric acid, *J. Atmos. Oceanic Technol.*, *23*, 1104–1113, doi:10.1175/JTECH1900.1.

Kleinman, L. I., P. H. Daum, Y.-N. Lee, L. J. Nunnermacker, S. R. Springston, J. W. Weinstein-Lloyd, and J. Rudolph (2005), A comparative study of ozone production in five U.S. metropolitan areas, *J. Geophys. Res.*, *110*, D02301, doi:10.1029/2004JD005096.

Koike, M., et al. (2003), Export of anthropogenic reactive nitrogen and sulfur compounds from the East Asia region in spring, *J. Geophys. Res.*, *108*(D20), 8789, doi:10.1029/2002JD003284.

Kondo, Y., et al. (1997), Profiles and partitioning of reactive nitrogen over the Pacific Ocean in winter and early spring, *J. Geophys. Res.*, *102*, 28,405–28,424.

Kondo, Y., et al. (2004), Impact of biomass burning in Southeast Asia on ozone and reactive nitrogen over the western Pacific in spring, *J. Geophys. Res.*, *109*, D15S12, doi:10.1029/2003JD004203.

Kondo, Y., et al. (2006), Temporal variations of elemental carbon in Tokyo, *J. Geophys. Res.*, *111*, D12205, doi:10.1029/2005JD006257.

Kondo, Y., Y. Miyazaki, N. Takegawa, T. Miyakawa, R. J. Weber, J. L. Jimenez, Q. Zhang, and D. R. Worsnop (2007), Oxygenated and water-soluble organic aerosols in Tokyo, *J. Geophys. Res.*, *112*, D01203, doi:10.1029/2006JD007056.

Kondo, Y., et al. (2008), Mechanisms that influence the formation of high-ozone regions in the boundary layer downwind of the Asian continent in winter and spring, *J. Geophys. Res.*, *113*, D15304, doi:10.1029/2007JD008978.

Marr, L. C., D. R. Black, and R. A. Harley (2002), Formation of photochemical air pollution in central California: 1. Development of a revised motor vehicle emission inventory, *J. Geophys. Res.*, *107*(D6), 4047, doi:10.1029/2001JD000689.

McKenzie, R., P. Johnston, A. Hofzumahaus, A. Kraus, S. Madronich, C. Cantrell, J. Calvert, and R. Shetter (2002), Relationship between photolysis frequencies derived from spectroscopic measurement of actinic fluxes and irradiances during the IPMMI campaign, *J. Geophys. Res.*, *107*(D5), 4042, doi:10.1029/2001JD000601.

McKenzie, R. L., C. Weinreis, P. V. Johnston, B. Liley, H. Shiona, M. Kotkamp, D. Smale, N. Takegawa, and Y. Kondo (2008), Effects of urban pollution on UV spectral irradiance, *Atmos. Chem. Phys.*, *8*, 5683–5697.

Miguel, A. H., T. W. Kirchstetter, and R. A. Harley (1998), On-road emissions of particulate polycyclic aromatic hydrocarbons and black carbon from gasoline and diesel vehicles, *Environ. Sci. Technol.*, *32*, 450–455, doi:10.1021/es970566w.

Miyakawa, T., N. Takegawa, and Y. Kondo (2008), Photochemical evolution of submicron aerosol chemical composition in the Tokyo megacity region in summer, *J. Geophys. Res.*, *113*, D14304, doi:10.1029/2007JD009493.

Miyazaki, Y., et al. (2005), Contribution of particulate nitrate to airborne measurements of total reactive nitrogen, *J. Geophys. Res.*, *110*, D15304, doi:10.1029/2004JD005502.

Molina, L. T., and M. J. Molina (1986), Absolute absorption cross-sections of ozone in the 185 to 350 nm wavelength range, *J. Geophys. Res.*, *91*(D13), 14,501–14,508.

Morino, Y., Y. Kondo, N. Takegawa, Y. Miyazaki, K. Kita, Y. Komazaki, M. Fukuda, T. Miyakawa, N. Moteki, and D. R. Worsnop (2006), Partitioning of HNO_3 and particulate nitrate over Tokyo: Effect of vertical mixing, *J. Geophys. Res.*, *111*, D15215, doi:10.1029/2005JD006887.

Murayama, T., H. Okamoto, N. Kaneyasu, H. Kamataki, and K. Miura (1999), Application of lidar depolarization measurement in the atmospheric boundary layer: Effects of dust and sea-salt particles, *J. Geophys. Res.*, *104*, 31,781–31,792.

Nakamura, K., et al. (2003), Measurement of NO_2 by photolysis conversion technique during TRACE-P, *J. Geophys. Res.*, *108*(D24), 4752, doi:10.1029/2003JD003712.

Neuman, J. A., et al. (2002), Fast-response airborne in situ measurements of HNO_3 during the Texas 2000 Air Quality Study, *J. Geophys. Res.*, *107*(D20), 4436, doi:10.1029/2001JD001437.

Neuman, J. A., D. D. Parrish, T. B. Ryerson, C. A. Brock, C. Wiedinmyer, G. J. Frost, J. S. Holloway, and F. C. Fehsenfeld (2004), Nitric acid loss rates measured in power plant plumes, *J. Geophys. Res.*, *109*, D23304, doi:10.1029/2004JD005092.

Nunnermacker, L. J., et al. (1998), Characterization of the Nashville urban plume on July 3 and July 18, 1995, *J. Geophys. Res.*, *103*(D21), 28,129–28,148.

Nunnermacker, L. J., K. I. Kleinman, D. Imre, P. H. Daum, Y.-N. Lee, J. H. Lee, S. R. Springston, and L. Newman (2000), NO_y lifetimes and O_3 production efficiencies in urban and power plant plumes: Analysis of field data, *J. Geophys. Res.*, *105*, 9165–9176.

O'Brien, J. M., P. B. Shepson, Q. Wu, T. Biesenthal, J. W. Bottenheim, H. A. Wiebe, K. G. Anlauf, and P. Brickell (1997), Production and distribution of organic nitrates, and their relationship to carbonyl compounds in an urban environment, *Atmos. Environ.*, *31*, 2059–2069, doi:10.1016/S1352-2310(97)80002-7.

Odum, J. R., T. P. W. Jungkamp, R. J. Griffin, R. C. Flagan, and J. H. Seinfeld (1997), The atmospheric aerosol-forming potential of whole gasoline vapor, *Science*, *276*, 96–99, doi:10.1126/science.276.5309.96.

Parrish, D. D., et al. (1993), The total reactive oxidized nitrogen levels and the partitioning between the individual species at six rural sites in eastern North America, *J. Geophys. Res.*, *98*, 2927–2939.

Parrish, D. D., M. Trainer, J. S. Holloway, J. E. Yee, M. S. Warshawsky, and F. C. Fehsenfeld (1998), Relationships between ozone and carbon monoxide at surface sites in the North Atlantic region, *J. Geophys. Res.*, *103*, 13,357–13,376.

Parrish, D. D., M. Trainer, D. Hereid, E. J. Williams, K. J. Olszyna, R. A. Harley, J. F. Meagher, and F. C. Fehsenfeld (2002), Decadal change in carbon monoxide to nitrogen oxide ratio in U.S. vehicular emissions, *J. Geophys. Res.*, *107*(D12), 4140, doi:10.1029/2001JD000720.

Ramanathan, V., et al. (2007), Atmospheric brown clouds: Hemispherical and regional variations in long-range transport, absorption, and radiative forcing, *J. Geophys. Res.*, *112*, D22S21, doi:10.1029/2006JD008124.

Ridley, B. A., J. G. Walega, J.-F. Lamarque, F. E. Grahek, M. Trainer, G. Hubler, X. Lin, and F. C. Fehsenfeld (1998), Measurements of reactive nitrogen and ozone to 5-km altitude in June 1990 over the southeastern United States, *J. Geophys. Res.*, *103*, 8369–8388.

Roberts, J. M., et al. (2001), Observations of APAN during TexAQS 2000, *Geophys. Res. Lett.*, *28*, 4195–4198.

Rosen, R. S., E. C. Wood, P. J. Wooldridge, J. A. Thornton, D. A. Day, W. Kuster, E. J. Williams, B. T. Jobson, and R. C. Cohen (2004), Observations of total alkyl nitrates during Texas Air Quality Study 2000: Implications for O_3 and alkyl nitrate photochemistry, *J. Geophys. Res.*, *109*, D07303, doi:10.1029/2003JD004227.

Ryerson, T. R., et al. (1998), Emission lifetimes and ozone formation in power plant plumes, *J. Geophys. Res.*, *103*, 22,569–22,583.

Ryerson, T. R., et al. (2003), Effect of photochemical industrial emissions of reactive alkenes and NO_x on tropospheric ozone formation in Houston, Texas, *J. Geophys. Res.*, *108*(D8), 4249, doi:10.1029/2002JD003070.

Sawyer, R. F., R. A. Harley, S. H. Cadle, J. M. Norbeck, R. Slott, and H. A. Bravo (2000), Mobile sources critical review: 1998 NARSTO assessment, *Atmos. Environ.*, *34*, 2161–2181, doi:10.1016/S1352-2310(99)00463-X.

Seinfeld, J. H., and S. N. Pandis (2006), *Atmospheric Chemistry and Physics: From Air Pollution to Climate Change*, 1203 pp., John Wiley, New York.

Shirai, T., Y. Yokouchi, D. R. Blake, K. Kita, K. Izumi, M. Koike, Y. Komazaki, Y. Miyazaki, M. Fukuda, and Y. Kondo (2007), Seasonal variations of atmospheric C_2-C_7 nonmethane hydrocarbons in Tokyo, *J. Geophys. Res.*, *112*, D24305, doi:10.1029/2006JD008163.

Sillman, S. (1999), The relation between ozone, NO_x, and hydrocarbons in urban and polluted rural environments, *Atmos. Environ.*, *33*, 1821–1845, doi:10.1016/S1352-2310(98)00345-8.

Simpson, I. J., et al. (2003), Photochemical production and evolution of selected C_2–C_5 alkyl nitrates in tropospheric air influenced by Asian outflow, *J. Geophys. Res.*, *108*(D20), 8808, doi:10.1029/2002JD002830.

Singh, H. B., L. J. Salas, and W. Viezee (1986), Global distribution of peroxyacetyl nitrate, *Nature*, *321*, 588–591, doi:10.1038/321588a0.

Spokes, L. J., S. G. Yeatman, S. E. Cornell, and T. D. Jickells (2000), Nitrogen deposition to the eastern Atlantic Ocean: The importance of south-easterly flow, *Tellus, Ser. B*, *52*, 37–49, doi:10.1034/j.1600-0889.2000.00062.x.

Stockwell, W. R., F. Kirchner, M. Kuhn, and S. Seefeld (1997), A new mechanism for regional atmospheric chemistry modeling, *J. Geophys. Res.*, *102*, 25,847–25,879.

Sullivan, A. P., R. E. Peltier, C. A. Brock, J. A. de Gouw, J. S. Holloway, C. Warneke, A. G. Wollny, and R. J. Weber (2006), Airborne measurements of carbonaceous aerosol soluble in water over northeastern United States: Method development and an investigation into water-soluble organic carbon sources, *J. Geophys. Res.*, *111*, D23S46, doi:10.1029/2006JD007072.

Takegawa, N., et al. (2004), Removal of NO_x and NO_y in Asian outflow plumes: Aircraft measurements over the western Pacific in January 2002, *J. Geophys. Res.*, *109*, D23S04, doi:10.1029/2004JD004866.

Takegawa, N., Y. Miyazaki, Y. Kondo, Y. Komazaki, T. Miyakawa, J. L. Jimenez, J. T. Jayne, D. R. Worsnop, J. D. Allan, and R. J. Weber (2005), Characterization of an Aerodyne Aerosol Mass Spectrometer (AMS): Intercomparison with other aerosol instruments, *Aerosol Sci. Technol.*, *39*, 760–770.

Takegawa, N., T. Miyakawa, Y. Kondo, J. L. Jimenez, D. R. Worsnop, and M. Fukuda (2006a), Seasonal and diurnal variations of submicron organic aerosols in Tokyo observed using the Aerodyne aerosol mass spectrometer, *J. Geophys. Res.*, *111*, D11206, doi:10.1029/2005JD006515.

Takegawa, N., et al. (2006b), Evolution of submicron organic aerosol in polluted air exported from Tokyo, *Geophys. Res. Lett.*, *33*, L15814, doi:10.1029/2006GL025815.

Tanimoto, A., and H. Akimoto (2001), A new peroxycarboxylic nitric anhydride identified in the atmosphere: CH_2 = CHC (O)OONO$_2$ (APAN), *Geophys. Res. Lett.*, *28*, 2831–2834.

Tanimoto, H., J. Hirokawa, Y. Kajii, and H. Akimoto (1999), A new measurement technique of peroxyacetyl nitrate at parts per trillion by volume levels: Gas chromatography/negative ion chemical ionization mass spectrometry, *J. Geophys. Res.*, *104*, 21,343–21,354.

Tanimoto, H., H. Furutani, S. Kato, J. Matsumoto, Y. Makide, and H. Akimoto (2002), Seasonal cycles of ozone and oxidized nitrogen species in Northeast Asia: 1. Impact of regional climatology and photochemistry observed during RISOTTO 1999–2000, *J. Geophys. Res.*, *107*(D24), 4747, doi:10.1029/2001JD001496.

Tanimoto, H., Y. Sawa, H. Matsueda, I. Uno, T. Ohara, K. Yamaji, and S. Yonemura (2005), Significant latitudinal gradient in the surface ozone spring maximum over East Asia, *Geophys. Res. Lett.*, *32*, L21805, doi:10.1029/2005GL023514.

Thornton, J. A., et al. (2002), Ozone production rates as a function of NO_x abundances and HO_x production rates in the Nashville urban plume, *J. Geophys. Res.*, *107*(D12), 4146, doi:10.1029/2001JD000932.

Tie, X., et al. (2003), Effect of sulfate aerosol on tropospheric NO_x and ozone budgets: Model simulations and TOPSE evidence, *J. Geophys. Res.*, *108*(D4), 8364, doi:10.1029/2001JD001508.

Wakamatsu, S., Y. Ogawa, K. Murano, K. Goi, and Y. Aburamoto (1983), Aircraft survey of the secondary photochemical pollutants covering the Tokyo metropolitan area, *Atmos. Environ.*, *17*(4), 827–835, doi:10.1016/0004-6981(83)90434-1.

Wakamatsu, S., T. Ohara, and I. Uno (1996), Recent trends in precursor concentrations and oxidant distributions in the Tokyo and Osaka areas, *Atmos. Environ.*, *30*(5), 715–721, doi:10.1016/1352-2310(95)00274-X.

Wakamatsu, S., I. Uno, T. Ohara, and K. L. Schere (1999), A study of the relationship between photochemical ozone and its precursor emissions of nitrogen oxides and hydrocarbons in Tokyo and surrounding areas, *Atmos. Environ.*, *33*(19), 3097–3108, doi:10.1016/S1352-2310(97)00493-7.

D. R. Blake, Department of Chemistry, University of California, Irvine, Irvine, CA 92697-2025, USA. (drblake@uci.edu)

M. Fukuda, Y. Kondo (corresponding author), and N. Takegawa, Research Center for Advanced Science and Technology, University of Tokyo, 4-6-1 Komaba, Meguro-ku, Tokyo 153-8904, Japan. (y.kondo@atmos.rcast.u-tokyo.ac.jp; takegawa@atmos.rcast.u-tokyo.ac.jp)

P. Johnston and R. McKenzie, National Institute of Water and Atmospheric Research, Lauder, Central Otago, New Zealand. (p.johnston@niwa.co.nz; r.mckenzie@niwa.co.nz)

Y. Kanaya, Frontier Research Center for Global Change, Japan Agency for Marine-Earth Science and Technology, 3173-25 Showa-machi, Kanazawa-ku, Yokohama, Kanagawa 236-0001, Japan. (yugo@jamstec.go.jp)

M. Koike, Department of Earth and Planetary Science, Graduate School of Science, University of Tokyo, Hongo 7-3-1, Bunkyo-ku, Tokyo 113-0033, Japan. (koike@eps.s.u-tokyo.ac.jp)

Y. Miyazaki, Institute of Low Temperature Science, Hokkaido University, Kita-19, Nishi-8, Kita-ku, Sapporo 060-0819, Japan. (yuzom@pop.lowtem.hokudai.ac.jp)

Y. Morino and H. Tanimoto, Asian Environment Research Group, National Institute for Environmental Studies, Tsukuba, Ibaraki 305-8506, Japan. (morino.yu@nies.go.jp; tanimoto@nies.go.jp)

T. Murayama, Faculty of Marine Technology, Tokyo University of Marine Science and Technology, 2-1-6 Etchujima, Koto, Tokyo 135-8533, Japan. (murayama@e.kaiyodai.ac.jp)